Molecular Therapy
Original Article

Neuronal genetic rescue normalizes brain network dynamics in a lysosomal storage disorder despite persistent storage accumulation

Rebecca C. Ahrens-Nicklas,[1,2] Luis Tecedor,[3] Arron F. Hall,[2] Owen Kane,[2] Richard J. Chung,[2] Elena Lysenko,[3] Eric D. Marsh,[1,4,5] Colleen S. Stein,[6] and Beverly L. Davidson[3,7]

[1]Department of Pediatrics, Perelman School of Medicine at the University of Pennsylvania, Philadelphia, PA, USA; [2]Division of Human Genetics, The Children's Hospital of Philadelphia, Philadelphia, PA, USA; [3]The Raymond G. Perelman Center for Cellular and Molecular Therapeutics, The Children's Hospital of Philadelphia, Philadelphia, PA, USA; [4]Department of Neurology, Perelman School of Medicine at the University of Pennsylvania, Philadelphia, PA, USA; [5]Division of Child Neurology, The Children's Hospital of Philadelphia, Philadelphia, PA, USA; [6]Department of Internal Medicine, Fraternal Order of Eagles Diabetes Research Center, Abboud Cardiovascular Research Center, Carver College of Medicine, University of Iowa, Iowa City, IA, USA; [7]The Department of Pathology and Laboratory Medicine, Perelman School of Medicine at the University of Pennsylvania, Philadelphia, PA, USA

Although neurologic symptoms occur in two-thirds of lysosomal storage disorders (LSDs), for most we do not understand the mechanisms underlying brain dysfunction. A major unanswered question is if the pathogenic hallmark of LSDs, storage accumulation, induces functional defects directly or is a disease bystander. Also, for most LSDs we do not know the impact of loss of function in individual cell types. Understanding these critical questions are essential to therapy development. Here, we determine the impact of genetic rescue in distinct cell types on neural circuit dysfunction in CLN3 disease, the most common pediatric dementia and a paradigmatic neurodegenerative LSD. We restored *Cln3* expression via AAV-mediated gene delivery and conditional genetic rescue in a CLN3 disease mouse model. Surprisingly, we found that low-level rescue of Cln3 expression in neurons alone normalized clinically relevant electrophysiologic markers of network dysfunction, despite the presence of substantial residual histopathology, in contrast to restoring expression in astrocytes. Thus, loss of CLN3 function in neurons, not storage accumulation, underlies neurologic dysfunction in CLN3 disease. This impliesies that storage clearance may be an inappropriate target for therapy development and an ineffectual biomarker.

INTRODUCTION

Lysosomal storage disorders (LSDs) are a group of approximately 50 rare metabolic diseases characterized by progressive accumulation of storage material in lysosomes. Neurological symptoms, including neurocognitive regression, seizures, and psychiatric symptoms, occur in more than two-thirds of LSDs and are generally not ameliorated by current therapies.[1] For many LSDs, including CLN3 disease, the most common cause of childhood dementia, the mechanisms underlying neurologic dysfunction are poorly understood.

The function of CLN3 protein remains unknown, hindering mechanism-based therapy development. The brains of CLN3 disease mouse models demonstrate progressive storage accumulation, predominantly comprised of subunit C of the mitochondrial ATP synthase (SCMAS),[2,3] mirroring what occurs in CLN3 disease patients.[4] Therefore, most drug development efforts rely on histopathologic markers of efficacy, including reduction of storage material, reactive astrocytosis, and microgliosis.[5–7] However, whether these histopathologic changes cause disease, augment the disease process, or are simply harmless epiphenomenon, is unclear.

In addition to lack of clarity on the impact of storage, the role of various central nervous system (CNS) cell types in driving functional deficits in CLN3 disease is unknown. Astrocytes and microglia isolated from CLN3 disease mouse models demonstrate altered cellular properties and physiology[8–10] and, in animal models, localized glial activation occurs in regions where neurons will later die[11] supporting a role for glia as a disease driver. On the other hand, neurons from CLN3 animal models exhibit both histopathologic and functional differences.[2,12,13] Ultimately, patients' symptoms, such as seizures and neurologic regression, arise directly from activity changes in key neuronal circuits, i.e., neuronal network dysfunction. Nonetheless, we do not understand what cell types underlie these pathologic network dynamics in the brain.

Previously, we described network-level neurologic defects in both the cortex and hippocampus of two CLN3 disease mouse models using *in vitro* voltage-sensitive dye imaging and *in vivo* electrophysiology

Received 10 September 2021; accepted 31 March 2022;
https://doi.org/10.1016/j.ymthe.2022.03.025.

Correspondence: Rebecca C. Ahrens-Nicklas, MD, PhD, Division of Human Genetics, The Children's Hospital of Philadelphia, 3501 Civic Center Blvd, 5014 CTRB, Philadelphia, PA 19104, USA.
E-mail: ahrensnicklasr@email.chop.edu
Correspondence: Beverly L. Davidson, PhD, The Raymond G. Perelman Center for Cellular and Molecular Therapeutics, The Children's Hospital of Philadelphia, 3501 Civic Center Boulevard, 5060 CTRB, Philadelphia, PA 19104, USA.
E-mail: davidsonbl@chop.edu

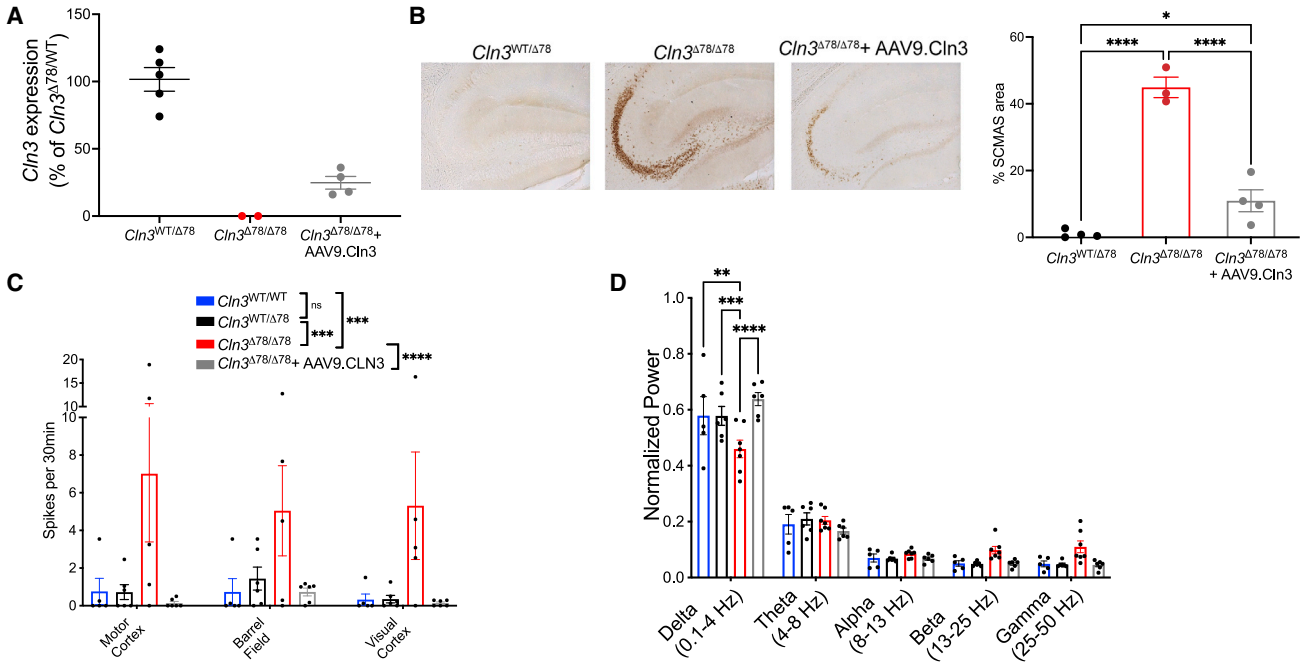

Figure 1. Intracerebroventricular AAV9.*Cln3* gene therapy given at p0 normalizes neuronal network dynamics *in vivo* at age 12 months

(A) p0 ICV injection of AAV9.*Cln3* restored *Cln3* expression in $Cln3^{\Delta ex78/\Delta ex78}$ mouse brain at age 12 months, with levels in the $Cln3^{\Delta ex78/\Delta ex78}$ hemisphere contralateral to the injection site reaching 24.5% ± 4.7% of heterozygous controls. (B) Subunit C of the mitochondrial ATP synthase (SCMAS) accumulation is partially prevented in the hippocampus ipsilateral to the injection site of $Cln3^{\Delta ex78/\Delta ex78}$ mice treated with AAV9.*Cln3* (n = 3–4 mice, one-way ANOVA, followed by Tukey's multiple comparisons test). Gene replacement corrects circuit function measured on intracranial EEG, including (C) epileptiform spiking rates throughout the cortex and (D) background frequency band composition in the motor cortex. Groups: $Cln3^{WT/WT}$ (blue); $Cln3^{WT/\Delta ex78}$ (black); $Cln3^{\Delta ex78/\Delta ex78}$ (red); $Cln3^{\Delta ex78/\Delta ex78}$ + AAV9.CLN3 (gray). N = 5–6 animals/condition. Results from 12 h of recordings were averaged for each animal shown as an individual circle. Spikes were analyzed by two-way ANOVA, followed by Tukey's multiple comparisons test to compare between genotype groups. Frequency bands were analyzed by two-way ANOVA by band and genotype, followed by Tukey's multiple comparisons test (significant results of multiple comparison testing shown as *p < 0.05, **p < 0.01, ***p < 0.001, ****p < 0.0001). Data are shown as mean ± SEM.

techniques.[14] While many brain regions are affected in CLN3 disease, the cortex and hippocampus are especially vulnerable and show early pathologic changes in mouse models and human patients.[3,4,13,15]

We found that network-level changes begin early in the disease course before substantial storage accumulation in both the hippocampus and cortex. In slice recordings, these changes include hypoexcitability of the dentate gyrus of the hippocampus, a region essential for learning and memory. On *in vivo* electroencephalogram (EEG), CLN3 disease mice show frequent epileptiform spikes, a feature of many epilepsy models, and a shift toward high-frequency background activity, a change associated with cognitive impairment and present in Alzheimer's disease models and patients.[16,17]

To date, CLN3 disease research has been hindered by the fact that animal models have only subtle behavioral and survival phenotypes.[18,19] Most manifest histopathologic changes, including storage accumulation and reactive astrocytosis; however, these phenotypes may not correlate with CNS dysfunction. Our network-level electrophysiologic approach provides a robust, clinically meaningful measure of neurologic function that can be used to probe disease mechanisms and evaluate potential therapies.

Here, we developed a new "conditional rescue" mouse model of CLN3 disease. The model is homozygous for the most common human CLN3 disease mutation,[2] but also carries one copy of a Cre-inducible wild-type *Cln3* transgene, under the control of its endogenous promoter, allowing for cell-type-specific rescue of expression. We employed AAV-mediated gene replacement as a second strategy to restore *Cln3* expression and combined these tools with network-level electrophysiology techniques to answer three essential questions: (1) Does gene replacement correct neural circuit dysfunction in a LSD? (2) What cell types must be corrected to improve network dynamics? (3) Does storage accumulation underlie deficits in CNS network dynamics in CLN3 disease?

RESULTS

In previous work, we found that CLN3 disease mouse models demonstrate robust, progressive neuronal network defects.[14] We first assessed if neonatal correction of most CNS cell types could prevent circuit-level functional pathology. For this, we employed an adeno-associated virus serotype 9 (AAV9) vector expressing wild-type murine *Cln3* under control of 1,665 bp of the endogenous *Cln3* promoter, which mimics the low levels of expression seen in the endogenous setting (Figures S1 and S2; supplemental methods). The vector was delivered

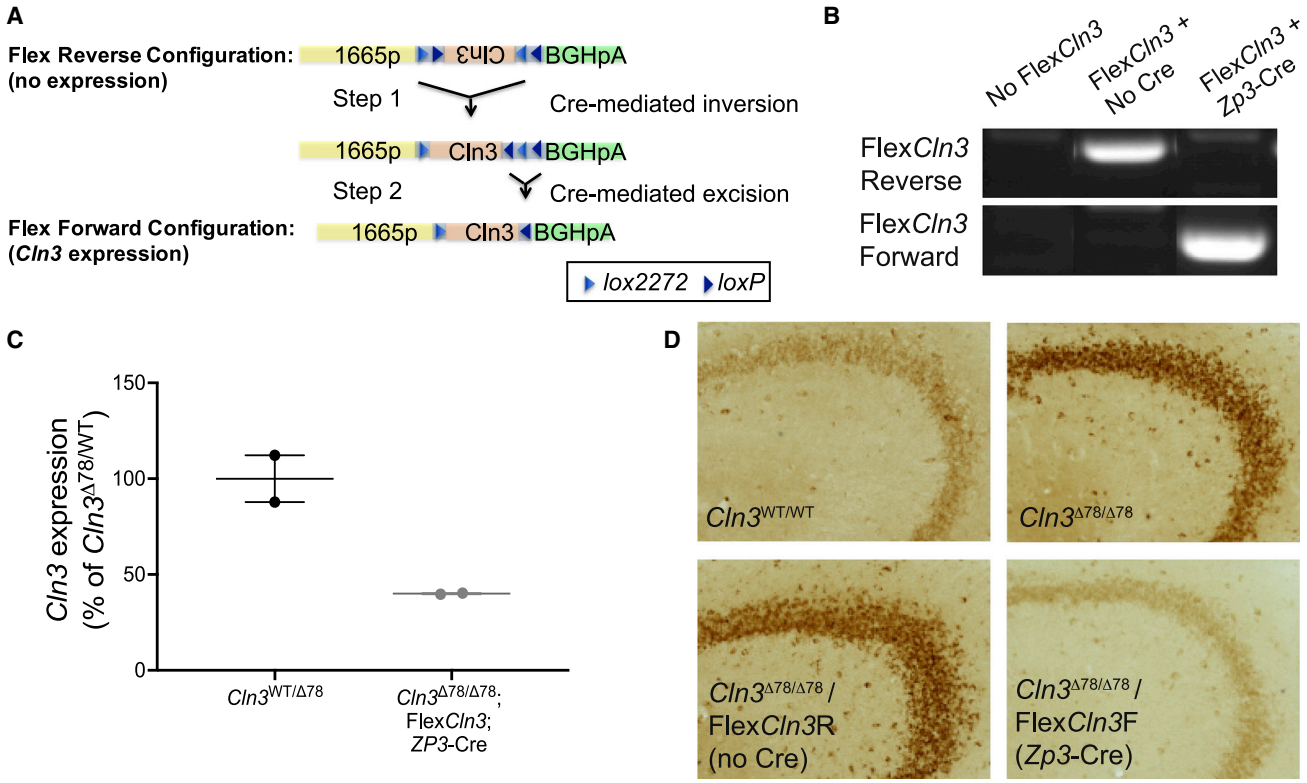

Figure 2. Expression of Flex*Cln3* allele in all cells reduces storage accumulation in *Cln3*$^{\Delta ex78/\Delta ex78}$ brain

(A) In the presence of Cre, the Flex*Cln3* allele undergoes inversion (step 1) and excision (step 2) and is expressed under control of its endogenous promoter. (B) PCR of genomic DNA from the hippocampus using orientation-specific primers confirms that the Flex*Cln3* is in the forward orientation only in the presence of Cre (see Figure S7 for uncut gels). (C) In the presence of *Zp3*-Cre, which drives ubiquitous recombination, the Flex*Cln3* allele results in expression levels that are 40.0% ± 0.4% of heterozygous controls. (D) Subunit C of the mitochondrial ATP synthase (SCMAS) accumulates in the hippocampus of *Cln3*$^{\Delta ex78/\Delta ex78}$ and Flex*Cln3*/*Cln3*$^{\Delta ex78/\Delta ex78}$ mice. Storage is reduced in mice with the Flex*Cln3* allele in the forward confirmation.

at p0 via unilateral intracerebroventricular (ICV) injection into CLN3-deficient mice to transduce both astrocytes and neurons[20] (Figure S3). The CLN3 disease mouse model harbors the most common human CLN3 disease mutation, a deletion of exons 7 and 8 (*Cln3*$^{\Delta ex78/\Delta ex78}$) (*2*). ICV injection of AAV9.*Cln3* at a dose of 1e^{10} vg increased *Cln3* expression (Figure 1A). One year after injection, levels in the *Cln3*$^{\Delta ex78/\Delta ex78}$ hemisphere contralateral to the injection site reached 24.5% ± 4.7% of heterozygous controls. When assessed histologically, gene replacement partially prevented storage accumulation in both the hippocampus and motor cortex ipsilateral to the injection site (Figures 1B and S4).

To determine the impact of p0 AAV9.*Cln3* infusion on *in vivo* network dynamics, we recorded activity throughout the brain via *in vivo* EEG. Twelve-month-old *Cln3*$^{\Delta ex78/\Delta ex78}$ mice have increased spike burden and a shift in background activity toward faster frequencies, with increased power in faster frequency bands compared with *Cln3*$^{WT/WT}$ and *Cln3*$^{\Delta ex78/WT}$ controls (Figures 1C and 1D). Specifically, there is decreased power in the slow delta frequency band (0.1–4 Hz) and a trend toward increased power in the faster beta (13–25 Hz) and gamma (25–50 Hz) bands in *Cln3*$^{\Delta ex78/\Delta ex78}$ mice, consistent with our previous report in *Cln3* knockout mice.[14] Remarkably, restoring gene expression at p0 normalized spiking rates (Figure 1C) and corrected background activity (Figure 1D) in 12-month-old *Cln3*$^{\Delta ex78/\Delta ex78}$ AAV9.*Cln3*-treated animals. Correction of EEG phenotypes was equally effective in both the hemispheres. Thus, early gene replacement can normalize network dynamics, and this rescue does not require full inhibition of storage accumulation.

Because AAV9 delivered to neonates transduces astrocytes and neurons,[20] it is unclear whether all cell types must be corrected to improve circuit function, a question critically important to translate gene therapies to children. AAV9 delivered into the CNS of different aged rodents and large animal models transduces different cell populations.[21–23] To address this, we developed a conditional rescue model of CLN3 disease, the Flex*Cln3* mouse. This model is homozygous for the common *Cln3* exon 7–8 deletion and also carries one Cre-inducible Flex*Cln3* allele, permitting expression of wild-type CLN3 protein in the presence of Cre recombinase (Figures 2 and S5–S7; supplemental methods). The Flex*Cln3* allele is under control of the same 1,665 bp *Cln3* promoter as used for AAV-mediated gene replacement.

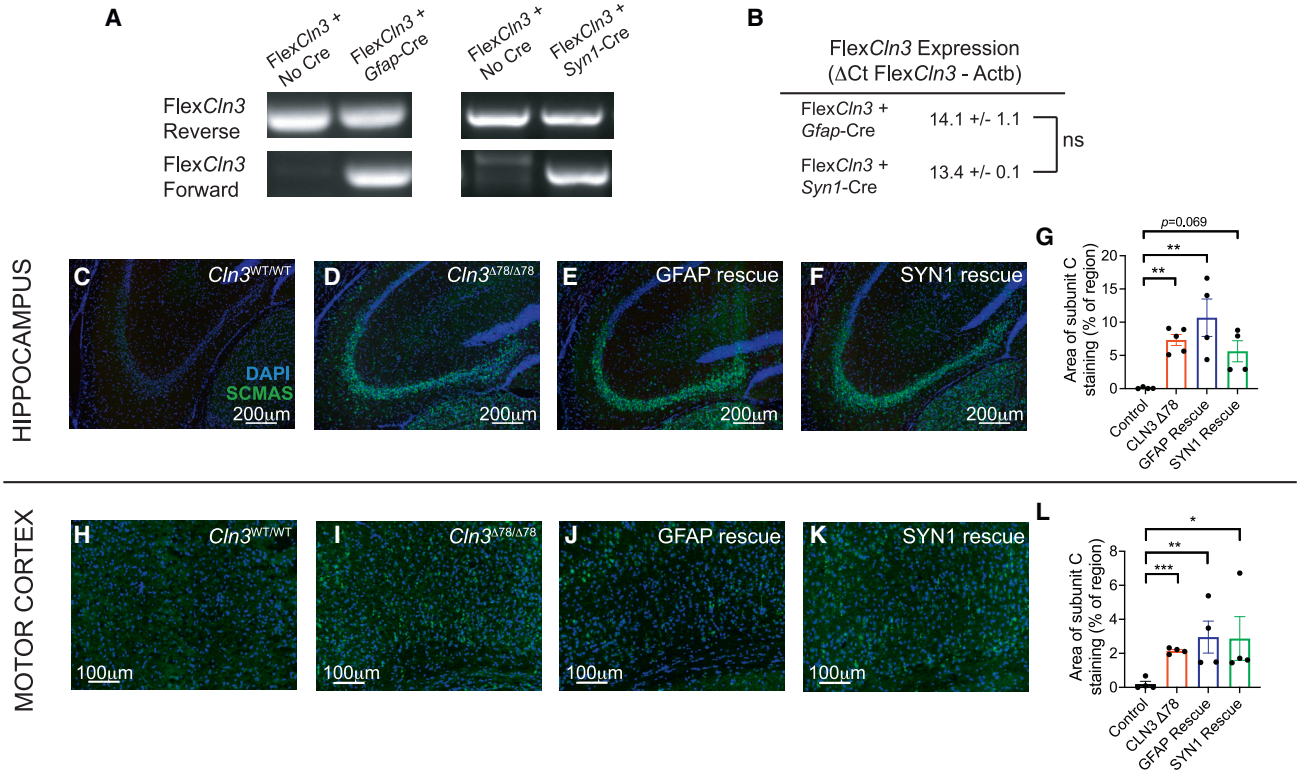

Figure 3. Expression of Flex*Cln3* allele in either neurons or astrocytes alone does not prevent storage accumulation in 12-month-old animals

(A) In the presence of Cre, the Flex*Cln3* allele undergoes inversion as detected by PCR with orientation-specific primers of genomic DNA from hippocampus. As both the *Gfap*-Cre and *Syn1*-Cre only drive recombination in a subset of cells, both the forward and reverse alleles are detected (see Figure S7 for uncut gels). (B) Expression levels as measured by ΔCt values (FlexCln3-βactin) are similar in Flex*Cln3* brain in the presence of *Gfap*-Cre and *Syn1*-Cre (14.1 versus 13.4, p = 0.53 by unpaired t test). (C–G) Expression of Flex*Cln3* in astrocytes (Flex*Cln3*/*Cln3*$^{\Delta ex78/\Delta ex78}$/*Gfap*-Cre animals) or neurons alone (Flex*Cln3*/*Cln3*$^{\Delta ex78/\Delta ex78}$/*Syn1*-Cre animals) does not prevent accumulation of SCMAS (green). (H–L) Similar findings were seen in the motor cortex. N = 4–5 animals, non-parametric Kruskal-Wallis test followed by Benjamini and Hochberg multiple comparisons correction to detect differences from control. For all panels: *p < 0.05, **p < 0.01, ***p < 0.001, ****p < 0.0001.

We validated the model by crossing Flex*Cln3* mice with *Zp3*-Cre mice[24] to drive germline level recombination and flip the reverse-oriented wild-type Flex*Cln3* allele into the forward orientation in all cells. Recombination of the allele was confirmed using orientation-specific PCR primers on genomic DNA extracted from the hippocampus (Figures 2B and S7). In these mice harboring a single Flex*Cln3* allele, expression was ubiquitously restored in all cell types with expression levels dictated by the transgenic *Cln3* 1,665 bp promoter. *Cln3* expression in the hippocampus was restored to 40% of heterozygous (*Cln3*$^{\Delta ex78/WT}$) control levels as determined by qPCR (Figure 2C). Correction (i.e., expression of the Flex*Cln3* transgene) in all cell types (Flex*Cln3*/*Cln3*$^{\Delta ex78/\Delta ex78}$/*Zp3*-Cre) substantially reduced SCMAS storage in the hippocampus and other brain regions to levels similar to *Cln3*$^{\Delta ex78/WT}$ or *Cln3*$^{WT/WT}$ (Figures 2D, 1B, and S8).

For selective rescue of astrocytes or neurons, Flex*Cln3* mice were crossed to *Gfap*-Cre[25] or *Syn1*-Cre[26] driver lines, respectively. Cre-mediated rearrangement of the Flex*Cln3* allele was confirmed by PCR of genomic DNA extracted from the hippocampus using orientation-specific primers (Figure 3A). As Cre is only expressed in a subset of cells (either astrocytes or neurons), unlike in the case of *Zp3*-Cre (Figure 2B), both the forward and reverse alleles were detected in hippocampal tissue.

Expression of forward-oriented Flex*Cln3* transcripts was confirmed in the hippocampus of the astrocyte and neuronal-specific rescue models. As rescue did not occur in all cell types, and *Cln3* protomer activity and expression can vary between cells and be induced by disease pathology,[3] it is difficult to normalize expression levels to heterozygote controls. However, to get a relative sense of expression levels we compared the level of Flex*Cln3* transgene expression in the astrocyte-only and neuron-only rescue models. We found no differences in transcript levels (normalized ΔCT values of 14.1 versus 13.4, p = 0.53 by unpaired t test) between the groups (Figure 3B). As there are no available antibodies that can reliably detect endogenous levels of mouse Cln3 protein,[27] we could not assess protein expression.

We next determined the impact of cell-type-selective restoration of *Cln3* expression on histopathological readouts. Rescue of *Cln3* expression in either astrocytes (Flex*Cln3*/*Cln3*$^{\Delta ex78/\Delta ex78}$/*Gfap*-Cre)

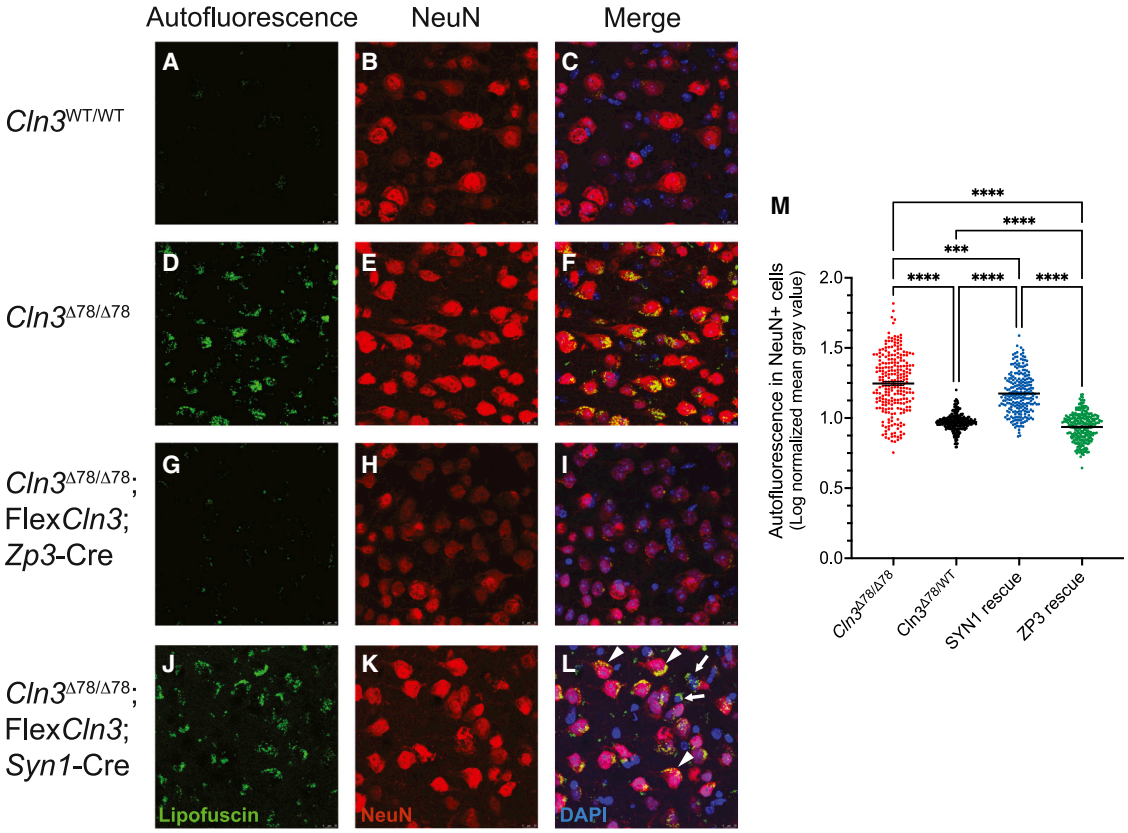

Figure 4. Expression of the Flex*Cln3* allele in neurons alone does not prevent autofluorescent lipofuscin accumulation in cortical neurons

(A–C) There is little autofluorescent lipofuscin accumulation (green) in wild-type cortical neurons (red) (blue DAPI) compared with (D–F) *Cln3*$^{\Delta 78/\Delta 78}$ cortical neurons in 12-month-old animals. (G–I) *Zp3*-Cre-induced expression of the Flex*Cln3* allele in all cell types prevents autofluorescent lipofuscin accumulation in both neuronal and non-neuronal cells. (J–L) Flex*Cln3* expression in neurons (*Syn1*-Cre) did not prevent storage accumulation in neurons (arrowheads) or non-neuronal cells (arrows). (M) Quantification of autofluorescence in neurons confirms storage accumulation in NeuN-positive cells after neuronal rescue. Three mice per group were analyzed with three images per mouse. Each image was fragmented for NeuN immunostaining, and autofluorescence was quantified in 238 or more NeuN-positive cells per group. Data represent mean gray value for each cell. Statistical analysis was performed with repeated measures one-way ANOVA followed by Sidak's multiple comparisons test. ***$p < 0.001$, ****$p < 0.0001$.

or neurons (Flex*Cln3*/*Cln3*$^{\Delta ex78/\Delta ex78}$/*Syn1*-Cre) alone did not prevent storage accumulation in the hippocampus or motor cortex in 6- or 12-month-old mice (Figures 3C–3L, S8, and S9). However, there may be region-specific differences as there was a partial reduction of storage in the thalamus after neuronal rescue (Figure S8).

In addition to storage accumulation, CLN3 disease mice develop progressive, reactive astrocytosis. At age 12 months, both the hippocampus and motor cortex of *Cln3*$^{\Delta ex78/\Delta ex78}$ showed increased astrocytosis compared with wild-type controls. Rescue of low-level *Cln3* expression in either neurons or astrocytes alone only partially improved astrocytosis (Figure S10), suggesting that higher level of expression to all cell types may be required to normalize astrocytosis.

To investigate if the Flex*Cln3* transgene could prevent storage accumulation in the specific cell type where it was expressed, we investigated colocalization of autofluorescent lipofuscin with a neuronal marker, NeuN, in cortical tissue (Figure 4). There is little lipofuscin accumulation in the *Cln3*$^{WT/WT}$ cortex compared with the *Cln3*$^{\Delta ex78/\Delta ex78}$ cortex, where there is storage in both neurons and non-neuronal cells. Ubiquitous Flex*Cln3* allele expression (in the presence of *Zp3*-Cre) prevented storage accumulation in all cell types. Flex*Cln3* allele expression in neurons (in the presence of *Syn1*-Cre) did not prevent storage in either neurons or non-neuronal cells.

Next, we determined if restoring *Cln3* expression could improve electrophysiologic measures despite residual storage accumulation. *In vitro* voltage-sensitive dye imaging of hippocampal slices from 6-month-old animals was completed in Flex*Cln3*/*Cln3*$^{\Delta ex78/\Delta ex78}$/*Gfap*-Cre, Flex*Cln3*/*Cln3*$^{\Delta ex78/\Delta ex78}$/*Syn1*-Cre, and Flex*Cln3*/*Cln3*$^{\Delta ex78/\Delta ex78}$/Zp3 mice. In this early stage of disease, the internal blade of the dentate gyrus of the *Cln3*$^{\Delta ex78/\Delta ex78}$ hippocampus was hypoexcitable in response to perforant path stimulation compared with heterozygous *Cln3*$^{\Delta 78/WT}$ mice (Figures 5A–5C), consistent with our previous studies.[14] Specifically, 31.6% of pixels in the internal blade of the *Cln3*$^{\Delta ex78/\Delta ex78}$ dentate gyrus were significantly hypoexcitable compared with slices obtained

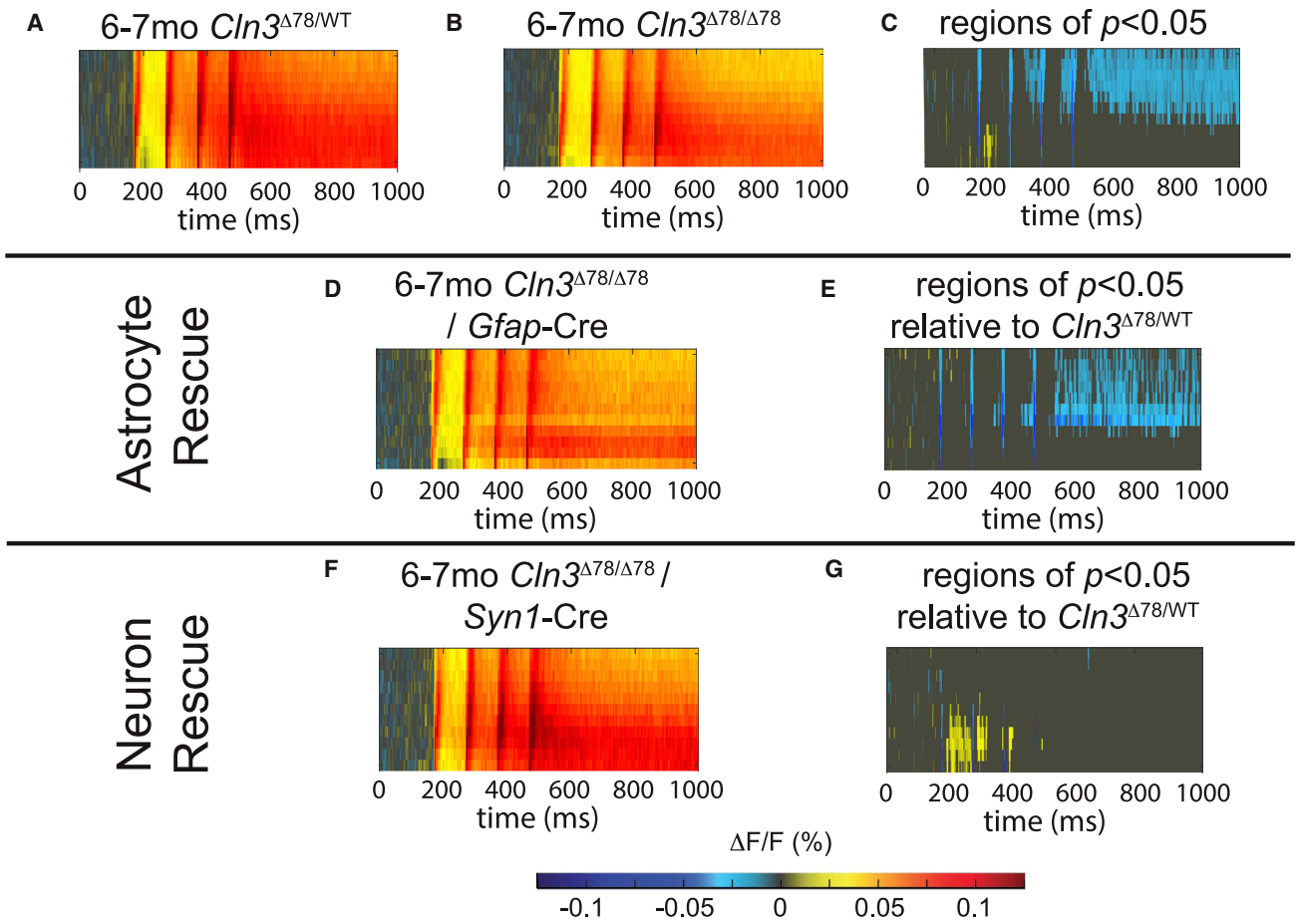

Figure 5. Restoring low-level *Cln3* expression in neurons alone corrects hypoexcitability of the dentate gyrus

Dentate gyrus excitability measured through *in vitro* voltage-sensitive dye imaging of hippocampal slices from 6-month-old animals is shown as raster plots of average fluorescence change (ΔF/F warm colors excitation, cool colors inhibition) over time (x axis) and location within the internal blade of the dentate gyrus (y axis). (A) Four-pulse stimulation of the perforant path in heterozygous control (*Cln3*$^{\Delta ex78/WT}$) mice reveals robust excitation of the dentate gyrus (DG) compared with (B) *Cln3*$^{\Delta ex78/\Delta ex78}$ mice. (C) *Cln3*$^{\Delta ex78/WT}$ versus *Cln3*$^{\Delta ex78/\Delta ex78}$ rasters were compared using a permutation sampling method with 1,000 trials. Pixels with $p > 0.05$ are masked in gray. For regions of significant difference in excitability with $p < 0.05$, the difference in fluorescence change ($\Delta F/F_{\Delta ex78/WT} - \Delta F/F_{\Delta ex78/\Delta ex78}$) is shown. (D and E) In animals expressing *Cln3* in astrocytes (Flex*Cln3*/*Cln3*$^{\Delta ex78/\Delta ex78}$/*Gfap*-Cre), the DG remained hypoexcitable compared with the *Cln3*$^{\Delta ex78/WT}$ DG. (F and G) Expression of *Cln3* in neurons alone (Flex*Cln3*/*Cln3*$^{\Delta ex78/\Delta ex78}$/*Syn1*-Cre) was sufficient to reverse hypoexcitability of the DG compared with *Cln3*$^{\Delta ex78/WT}$ animals. Group sizes (n = slices, N = mice): *Cln3*$^{\Delta ex78/WT}$ n = 23 N = 4; *Cln3*$^{\Delta ex78/\Delta ex78}$ n = 30, N = 6; Flex*Cln3*/*Cln3*$^{\Delta ex78/\Delta ex78}$/*Gfap-Cre* n = 19 slices, N = 4; Flex*Cln3*/*Cln3*$^{\Delta ex78/\Delta ex78}$/*Syn1-Cre* n = 17; N = 4.

from heterozygous control animals. Interestingly, restoring expression in astrocytes did not correct hypoexcitability of the dentate gyrus (Figures 5D and 5E), with 23.6% of pixels remaining hypoexcitable. However, restoring *Cln3* expression in neurons was sufficient to prevent disease-induced hypoexcitability (Figures 5F and 5G), reducing hypoexcitable pixels to 1% compared with heterozygous controls. This rescue of dynamics occurred despite the presence of residual histopathology (Figures 3, 4, and S8–S10).

To evaluate how cell-type-specific correction modulates CNS functional defects *in vivo*, we measured network activity through long-term EEG recordings. While restoration of *Cln3* expression in either astrocytes or neurons prevented epileptiform spikes throughout the brain (Figure 6A), only rescue in neurons corrected EEG background frequency composition (i.e., frequency band power) and thereby fully normalized network activity (Figures 6B–6F). Intriguingly, this correction of physiology occurred despite the presence of substantial storage burden, revealing for the first time that loss of CLN3 protein function in neurons, not storage burden, underlies functional defects in CLN3 disease.

DISCUSSION

Previous cellular-level studies of CLN3 disease have demonstrated disease-associated abnormalities in both neurons and astrocytes.[4,9–11,13,28–30] Prior to this work, it was unknown how these cellular defects translate to the circuit-level dysfunction that underlies neurological symptoms, such as dementia and seizures, that CLN3 disease patients experience. This work highlights the fact

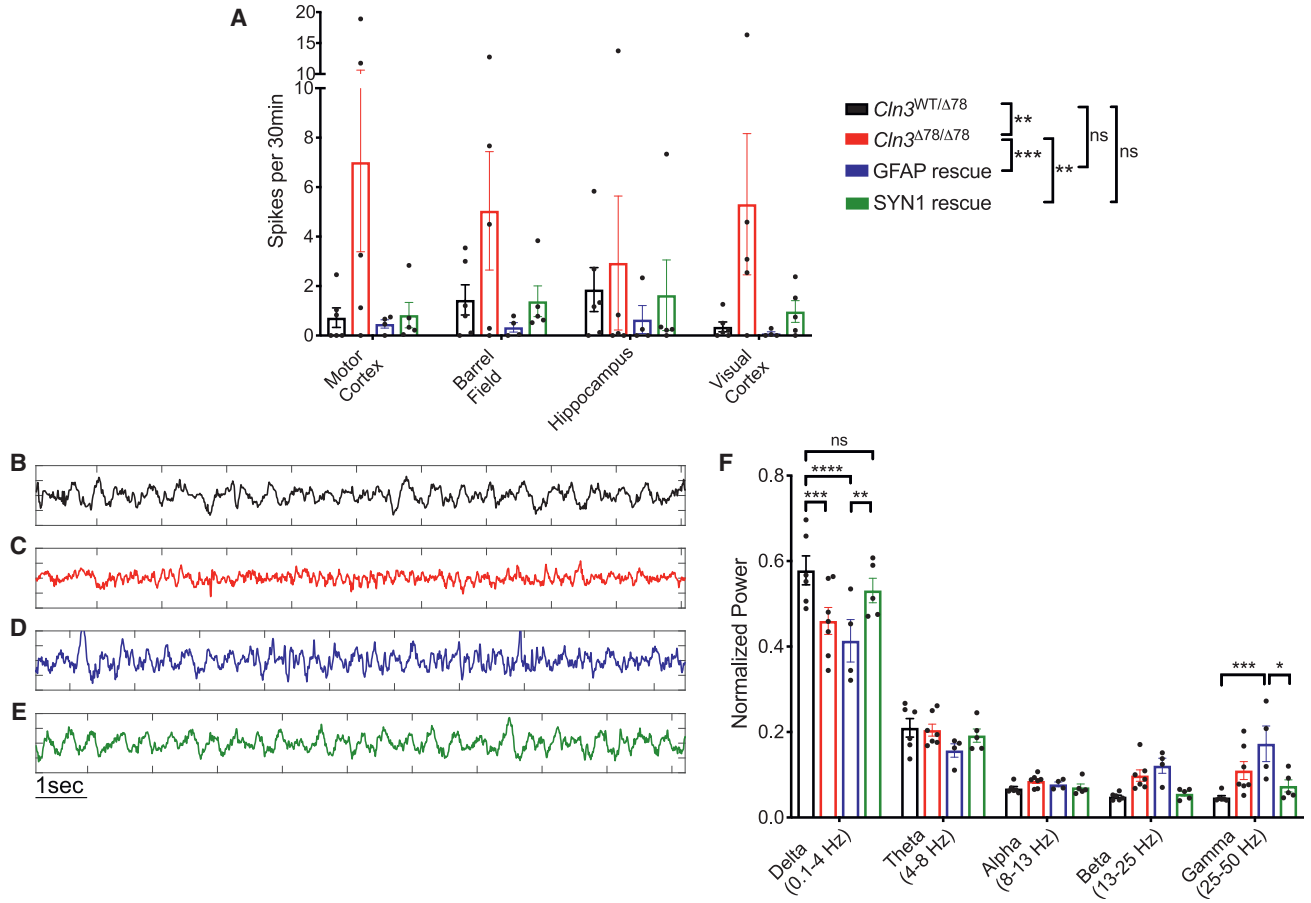

Figure 6. *Cln3* rescue in either astrocytes or neurons reduces epileptiform spikes, but only neuronal rescue fully normalizes network dynamics as measured on EEG

(A) Correction of either astrocytes (Flex*Cln3*/*Cln3*$^{\Delta ex78/\Delta ex78}$/*Gfap*-Cre, blue) or neurons (Flex*Cln3*/*Cln3*$^{\Delta ex78/\Delta ex78}$/*Syn1*-Cre, green) reduced spike burden on EEG in 12-month-old mice. (B–E) Example EEG traces from *Cln3*$^{\Delta ex78/\Delta ex78}$ (red) and Flex*Cln3*/*Cln3*$^{\Delta ex78/\Delta ex78}$/*Gfap*-Cre motor cortex (blue) show decreased slow delta activity and increased fast activity compared with control motor cortex (black). EEG trace from Flex*Cln3*/*Cln3*$^{\Delta ex78/\Delta ex78}$/*Syn1*-Cre motor cortex (green) shows that rescue of *Cln3* expression in neurons normalizes EEG background frequency composition. (F) Power spectral analysis of EEG data recorded in the motor cortex confirm that rescue of *Cln3* expression in astrocytes (blue) does not correct disease-associated loss of delta activity, and actually exacerbates increased fast gamma activity. However, correction in neurons (green) normalizes EEG frequency composition. N = 4–5 animals/genotype, after passing a Shapiro-Wilk test of normality, data were analyzed by two-way ANOVA, followed by Sidak's multiple comparisons test. Significant differences from multiple comparisons testing are shown as *p < 0.05, **p < 0.01, ***p < 0.001. Frequency data in (F) in *Cln3*$^{WT/\Delta ex78}$ and *Cln3*$^{\Delta ex78/\Delta ex78}$ are also shown in Figure 1D.

that neurons underlie network-level functional defects in CLN3 disease and must be targeted in future drug development efforts.

A number of novel therapies, including small molecule,[5,6,31–34] antisense oligonucleotides,[35] and gene replacement[7,36] strategies, are under development for CLN3 disease. These approaches will not target all cell types equally. For example, studies in non-human primates have demonstrated that intravenous administration of AAV9 in juvenile non-human primates predominately transduces glia,[23,37] while direct administration into the cerebral spinal fluid improves delivery to neurons.[34,38] Our results suggest that maximizing neuronal correction will be essential to develop a treatment that improves functional outcomes in CLN3 disease.

Future *in vitro* and *in vivo* studies evaluating different levels of rescue in a variety of cell types could provide further insights into how outcomes vary with level of gene expression rescue. In addition to neurons and astrocytes, Cln3 is expressed at low levels in other CNS cell types including endothelial cells and microglia.[39] Abnormalities in these cell types have been reported in CLN3 disease models.[6,10] Future investigations of *Cln3* rescue in these populations could further our understanding of disease mechanisms.

In previous studies, *Cln3*$^{\Delta ex78/\Delta ex78}$ mice have demonstrated abnormal astrocytic-neuronal coupling.[9] Monogenic mouse models of isolated astrocyte dysfunction have epileptiform spikes and seizures on EEG because of pathologic crosstalk between astrocytes

and neurons.[40] In the Flex*Cln3* mouse, rescue of *Cln3* expression in astrocytes alone actually exacerbated EEG background abnormalities, including increasing fast gamma activity. This suggests that balanced *Cln3* expression in both neurons and astrocytes may be required to maintain a normal EEG background. However, rescue in astrocytes alone was sufficient to prevent epileptiform spikes. The reduction in spiking likely reflects improved astrocytic-neuronal interactions when *Cln3* expression is restored in astrocytes. Collectively, our data suggest that diseased astrocytes may modulate network-level dysfunction in CLN3 disease, but diseased neurons are a primary driver of functional deficits.

Using our cell-type-specific rescue model, we found that storage accumulation was prevented when *Cln3* was reintroduced to all cell types embryonically, but not when that correction was restricted to astrocytes or neurons alone. Interestingly, prevention of storage accumulation is not required for correcting neuronal network physiology, suggesting that storage material may not be the primary driver of the disease process. This finding is consistent with a previous study of CLN3 gene therapy in mice, which demonstrated improvement in some disease markers despite residual storage accumulation.[7]

These studies highlight the importance of using clinically relevant functional measures, such as *in vivo* electrophysiology studies, to guide treatment development. Histologic measures, such as storage burden, may be incomplete surrogate biomarkers of therapeutic efficacy in CLN3 disease and possibly other neuronopathic LSDs. Future studies are needed to fully elucidate how loss of CLN3 protein in neurons leads to neurologic dysfunction. One emerging theory is that CLN3 may play a role in maintaining synaptic structure and function.[13,41,42] The circuit-level abnormalities demonstrated here could arise directly from these synaptic alterations, rather than in response to storage accumulation.

In summary, partial restoration of *Cln3* expression by AAV vectors or through Cre-based systems shows that neuronal expression is critical for preventing deficits in CNS functional circuits in CLN3 disease mice. This work also highlights that improvement in storage burden alone may not be an adequate readout of therapeutic efficacy in CLN3 disease, a phenomenon that should be considered by the broader LSD community.

MATERIALS AND METHODS

For additional information, see supplemental methods.

Study approval

All animal protocols were approved by the Institutional Animal Care and Use Committee at the Children's Hospital of Philadelphia.

Statistical analysis

All statistical analysis of VSDI rasters was completed using a permutation sampling method and the VSDI toolbox in MATLAB (The MathWorks) as described previously.[14,43] For summary statistics of regions or groups, GraphPad Prism was also used. In graphs, data are expressed as mean ± SEM. The statistical significance of the observed differences between two groups was assessed by two-tailed t test (for normally distributed data) or Mann-Whitney U test (for non-normally distributed data). For grouped datasets one- or two-way ANOVA followed by multiple comparisons test was completed as detailed in each figure legend. Results were considered significant when $p < 0.05$. Male and female mice were included in all groups.

SUPPLEMENTAL INFORMATION

Supplemental information can be found online at https://doi.org/10.1016/j.ymthe.2022.03.025.

ACKNOWLEDGMENTS

NINDS R21NS084424 and NICHD HD33532 to B.L.D., NIH K08NS105865 to R.C.A.-N., NCL Stiftung Research Award to R.C.A.-N., Chan Zuckerberg Initiative Neurodegeneration Challenge Network Award to R.C.A.-N., Children's Hospital of Philadelphia Research Institute support to R.C.A.-N. and B.L.D.

AUTHOR CONTRIBUTIONS

Design of study, R.C.A.-N., L.T., A.F.H., O.K., R.J.C., E.L., E.D.M., C.S.S., and B.L.D.; data acquisition and analysis of data, R.C.A.-N., L.T., A.F.H., O.K., R.J.C., E.L., and C.S.S.; drafting of the manuscript, R.C.A.-N., L.T., A.F.H., O.K., and C.S.S.; critical review of the data and manuscript, R.C.A.-N., L.T., E.D.M., C.S.S., and B.L.D.

DECLARATION OF INTERESTS

B.L.D. is a founder of Spark Therapeutics and Spirovant and is on the scientific advisory boards of Intellia Therapeutics, Homology Medicines, Prevail Therapeutics, Resilience, Moment Bio, Spirovant, Saliogen and Panorama Medicines. The other authors declare no competing interests.

REFERENCES

1. Platt, F.M. (2018). Emptying the stores: lysosomal diseases and therapeutic strategies. Nat. Rev. Drug Discov. *17*, 133–150. https://doi.org/10.1038/nrd.2017.214.

2. Cotman, S.L., Vrbanac, V., Lebel, L.A., Lee, R.L., Johnson, K.A., Donahue, L.R., Teed, A.M., Antonellis, K., Bronson, R.T., Lerner, T.J., and MacDonald, M.E. (2002). Cln3(Deltaex7/8) knock-in mice with the common JNCL mutation exhibit progressive neurologic disease that begins before birth. Hum. Mol. Genet. *11*, 2709–2721. https://doi.org/10.1093/hmg/11.22.2709.

3. Eliason, S.L., Stein, C.S., Mao, Q., Tecedor, L., Ding, S.L., Gaines, D.M., and Davidson, B.L. (2007). A knock-in reporter model of Batten disease. J. Neurosci. *27*, 9826–9834. https://doi.org/10.1523/JNEUROSCI.1710-07.2007.

4. Tyynela, J., Cooper, J.D., Khan, M.N., Shemilts, S.J., and Haltia, M. (2004). Hippocampal pathology in the human neuronal ceroid-lipofuscinoses: distinct patterns of storage deposition, neurodegeneration and glial activation. Brain Pathol. *14*, 349–357. https://doi.org/10.1111/j.1750-3639.2004.tb00077.x.

5. Tarczyluk-Wells, M.A., Salzlechner, C., Najafi, A.R., Lim, M.J., Smith, D., Platt, F.M., Williams, B.P., and Cooper, J.D. (2019). Combined anti-inflammatory and neuroprotective treatments have the potential to impact disease phenotypes in Cln3 (-/-) mice. Front. Neurol. *10*, 963. https://doi.org/10.3389/fneur.2019.00963.

6. Schultz, M.L., Tecedor, L., Lysenko, E., Ramachandran, S., Stein, C.S., and Davidson, B.L. (2018). Modulating membrane fluidity corrects Batten disease phenotypes *in vitro* and *in vivo*. Neurobiol. Dis. *115*, 182–193. https://doi.org/10.1016/j.nbd.2018.04.010.

7. Bosch, M.E., Aldrich, A., Fallet, R., Odvody, J., Burkovetskaya, M., Schuberth, K., Fitzgerald, J.A., Foust, K.D., and Kielian, T. (2016). Self-complementary AAV9 gene delivery partially corrects pathology associated with juvenile neuronal ceroid lipofuscinosis (CLN3). J. Neurosci. *36*, 9669–9682. https://doi.org/10.1523/JNEUROSCI.1635-16.2016.

8. Xiong, J., and Kielian, T. (2013). Microglia in juvenile neuronal ceroid lipofuscinosis are primed toward a pro-inflammatory phenotype. J. Neurochem. *127*, 245–258. https://doi.org/10.1111/jnc.12385.

9. Burkovetskaya, M., Karpuk, N., Xiong, J., Bosch, M., Boska, M.D., Takeuchi, H., Suzumura, A., and Kielian, T. (2014). Evidence for aberrant astrocyte hemichannel activity in juvenile neuronal ceroid lipofuscinosis (JNCL). PLoS One *9*, e95023. https://doi.org/10.1371/journal.pone.0095023.

10. Parviainen, L., Dihanich, S., Anderson, G.W., Wong, A.M., Brooks, H.R., Abeti, R., Rezaie, P., Lalli, G., Pope, S., Heales, S.J., et al. (2017). Glial cells are functionally impaired in juvenile neuronal ceroid lipofuscinosis and detrimental to neurons. Acta Neuropathol. Commun. *5*, 74. https://doi.org/10.1186/s40478-017-0476-y.

11. Pontikis, C.C., Cella, C.V., Parihar, N., Lim, M.J., Chakrabarti, S., Mitchison, H.M., Mobley, W.C., Rezaie, P., Pearce, D.A., and Cooper, J.D. (2004). Late onset neurodegeneration in the Cln3-/- mouse model of juvenile neuronal ceroid lipofuscinosis is preceded by low level glial activation. Brain Res. *1023*, 231–242. https://doi.org/10.1016/j.brainres.2004.07.030.

12. Brenneman, D.E., Pearce, D.A., Kovacs, A., and DeFrees, S. (2017). Pharmacological effects on ceroid lipofuscin and neuronal structure in Cln3 (ex7/8) mouse brain cultures. J. Mol. Neurosci. *63*, 100–114. https://doi.org/10.1007/s12031-017-0962-5.

13. Grunewald, B., Lange, M.D., Werner, C., O'Leary, A., Weishaupt, A., Popp, S., Pearce, D.A., Wiendl, H., Reif, A., Pape, H.C., et al. (2017). Defective synaptic transmission causes disease signs in a mouse model of juvenile neuronal ceroid lipofuscinosis. Elife *6*, e28685. https://doi.org/10.7554/eLife.28685.

14. Ahrens-Nicklas, R.C., Tecedor, L., Hall, A.F., Lysenko, E., Cohen, A.S., Davidson, B.L., and Marsh, E.D. (2019). Neuronal network dysfunction precedes storage and neurodegeneration in a lysosomal storage disorder. JCI Insight *4*, e131961. https://doi.org/10.1172/jci.insight.131961.

15. Mitchison, H.M., Lim, M.J., and Cooper, J.D. (2004). Selectivity and types of cell death in the neuronal ceroid lipofuscinoses. Brain Pathol. *14*, 86–96. https://doi.org/10.1111/j.1750-3639.2004.tb00502.x.

16. Kwak, Y.T. (2006). Quantitative EEG findings in different stages of Alzheimer's disease. J. Clin. Neurophysiol. *23*, 456–461. https://doi.org/10.1097/01.wnp.0000223453.47663.63.

17. Kent, B.A., Strittmatter, S.M., and Nygaard, H.B. (2018). Sleep and EEG power spectral analysis in three transgenic mouse models of Alzheimer's disease: APP/PS1, 3xTgAD, and Tg2576. J. Alzheimers Dis. *64*, 1325–1336. https://doi.org/10.3233/JAD-180260.

18. Faller, K.M., Gutierrez-Quintana, R., Mohammed, A., Rahim, A.A., Tuxworth, R.I., Wager, K., and Bond, M. (2015). The neuronal ceroid lipofuscinoses: opportunities from model systems. Biochim. Biophys. Acta *1852*, 2267–2278. https://doi.org/10.1016/j.bbadis.2015.04.022.

19. Johnson, T.B., Langin, L.M., Zhao, J., Weimer, J.M., Pearce, D.A., and Kovacs, A.D. (2019). Changes in motor behavior, neuropathology, and gut microbiota of a Batten disease mouse model following administration of acidified drinking water. Sci. Rep. *9*, 14962. https://doi.org/10.1038/s41598-019-51488-z.

20. Hammond, S.L., Leek, A.N., Richman, E.H., and Tjalkens, R.B. (2017). Cellular selectivity of AAV serotypes for gene delivery in neurons and astrocytes by neonatal intracerebroventricular injection. PLoS One *12*, e0188830. https://doi.org/10.1371/journal.pone.0188830.

21. Hinderer, C., Bell, P., Vite, C.H., Louboutin, J.P., Grant, R., Bote, E., Yu, H., Pukenas, B., Hurst, R., and Wilson, J.M. (2014). Widespread gene transfer in the central nervous system of cynomolgus macaques following delivery of AAV9 into the cisterna magna. Mol. Ther. Methods Clin. Dev. *1*, 14051. https://doi.org/10.1038/mtm.2014.51.

22. Gray, S.J., Nagabhushan Kalburgi, S., McCown, T.J., and Jude Samulski, R. (2013). Global CNS gene delivery and evasion of anti-AAV-neutralizing antibodies by intrathecal AAV administration in non-human primates. Gene Ther. *20*, 450–459. https://doi.org/10.1038/gt.2012.101.

23. Samaranch, L., Salegio, E.A., San Sebastian, W., Kells, A.P., Foust, K.D., Bringas, J.R., Lamarre, C., Forsayeth, J., Kaspar, B.K., and Bankiewicz, K.S. (2012). Adeno-associated virus serotype 9 transduction in the central nervous system of nonhuman primates. Hum. Gene Ther. *23*, 382–389. https://doi.org/10.1089/hum.2011.200.

24. Shafi, R., Iyer, S.P., Ellies, L.G., O'Donnell, N., Marek, K.W., Chui, D., Hart, G.W., and Marth, J.D. (2000). The O-GlcNAc transferase gene resides on the X chromosome and is essential for embryonic stem cell viability and mouse ontogeny. Proc. Natl. Acad. Sci. U S A *97*, 5735–5739. https://doi.org/10.1073/pnas.100471497.

25. Gregorian, C., Nakashima, J., Le Belle, J., Ohab, J., Kim, R., Liu, A., Smith, K.B., Groszer, M., Garcia, A.D., Sofroniew, M.V., et al. (2009). Pten deletion in adult neural stem/progenitor cells enhances constitutive neurogenesis. J. Neurosci. *29*, 1874–1886. https://doi.org/10.1523/JNEUROSCI.3095-08.2009.

26. Zhu, Y., Romero, M.I., Ghosh, P., Ye, Z., Charnay, P., Rushing, E.J., Marth, J.D., and Parada, L.F. (2001). Ablation of NF1 function in neurons induces abnormal development of cerebral cortex and reactive gliosis in the brain. Genes Dev. *15*, 859–876. https://doi.org/10.1101/gad.862101.

27. Nelson, T., Pearce, D.A., and Kovacs, A.D. (2017). Lack of specificity of antibodies raised against CLN3, the lysosomal/endosomal transmembrane protein mutated in juvenile Batten disease. Biosci. Rep. *37*. BSR20171229. https://doi.org/10.1042/BSR20171229.

28. Pontikis, C.C., Cotman, S.L., MacDonald, M.E., and Cooper, J.D. (2005). Thalamocortical neuron loss and localized astrocytosis in the Cln3Deltaex7/8 knock-in mouse model of Batten disease. Neurobiol. Dis. *20*, 823–836. https://doi.org/10.1016/j.nbd.2005.05.018.

29. Bosch, M.E., and Kielian, T. (2019). Astrocytes in juvenile neuronal ceroid lipofuscinosis (CLN3) display metabolic and calcium signaling abnormalities. J. Neurochem. *148*, 612–624. https://doi.org/10.1111/jnc.14545.

30. Zhong, Y., Mohan, K., Liu, J., Al-Attar, A., Lin, P., Flight, R.M., Sun, Q., Warmoes, M.O., Deshpande, R.R., Liu, H., et al. (2020). Loss of CLN3, the gene mutated in juvenile neuronal ceroid lipofuscinosis, leads to metabolic impairment and autophagy induction in retinal pigment epithelium. Biochim. Biophys. Acta Mol. Basis Dis. *1866*, 165883. https://doi.org/10.1016/j.bbadis.2020.165883.

31. Augustine, E.F., Beck, C.A., Adams, H.R., Defendorf, S., Vierhile, A., Timm, D., Weimer, J.M., Mink, J.W., and Marshall, F.J. (2019). Short-term administration of mycophenolate is well-tolerated in CLN3 disease (juvenile neuronal ceroid lipofuscinosis). JIMD Rep. *43*, 117–124. https://doi.org/10.1007/8904_2018_113.

32. El-Sitt, S., Soueid, J., Maalouf, K., Makhoul, N., Al Ali, J., Makoukji, J., Asser, B., Daou, D., Harati, H., and Boustany, R.M. (2019). Exogenous galactosylceramide as potential treatment for CLN3 disease. Ann. Neurol. *86*, 729–742. https://doi.org/10.1002/ana.25573.

33. Petcherski, A., Chandrachud, U., Butz, E.S., Klein, M.C., Zhao, W.N., Reis, S.A., Haggarty, S.J., Ruonala, M.O., and Cotman, S.L. (2019). An autophagy modifier screen identifies small molecules capable of reducing autophagosome accumulation in a model of CLN3-mediated neurodegeneration. Cells *8*, 1531. https://doi.org/10.3390/cells8121531.

34. Maalouf, K., Makoukji, J., Saab, S., Makhoul, N.J., Carmona, A.V., Kinarivala, N., Ghanem, N., Trippier, P.C., and Boustany, R.M. (2020). Exogenous flupirtine as potential treatment for CLN3 disease. Cells *9*, 1872. https://doi.org/10.3390/cells9081872.

35. Centa, J.L., Jodelka, F.M., Hinrich, A.J., Johnson, T.B., Ochaba, J., Jackson, M., Duelli, D.M., Weimer, J.M., Rigo, F., and Hastings, M.L. (2020). Therapeutic efficacy of antisense oligonucleotides in mouse models of CLN3 Batten disease. Nat. Med. *26*, 1444–1451. https://doi.org/10.1038/s41591-020-0986-1.

36. Kleine Holthaus, S.M., Aristorena, M., Maswood, R., Semenyuk, O., Hoke, J., Hare, A., Smith, A.J., Mole, S.E., and Ali, R.R. (2020). Gene therapy targeting the inner retina rescues the retinal phenotype in a mouse model of CLN3 batten disease. Hum. Gene Ther. *31*, 709–718. https://doi.org/10.1089/hum.2020.038.

37. Gray, S.J., Matagne, V., Bachaboina, L., Yadav, S., Ojeda, S.R., and Samulski, R.J. (2011). Preclinical differences of intravascular AAV9 delivery to neurons and glia: a comparative study of adult mice and nonhuman primates. Mol. Ther. *19*, 1058–1069. https://doi.org/10.1038/mt.2011.72.

38. Bey, K., Deniaud, J., Dubreil, L., Joussemet, B., Cristini, J., Ciron, C., Hordeaux, J., Le Boulc'h, M., Marche, K., Maquigneau, M., et al. (2020). Intra-CSF AAV9 and

AAVrh10 administration in nonhuman primates: promising routes and vectors for which neurological diseases? Mol. Ther. Methods Clin. Dev. *17*, 771–784. https://doi.org/10.1016/j.omtm.2020.04.001.

39. Yao, Z., van Velthoven, C.T.J., Nguyen, T.N., Goldy, J., Sedeno-Cortes, A.E., Baftizadeh, F., Bertagnolli, D., Casper, T., Chiang, M., Crichton, K., et al. (2021). A taxonomy of transcriptomic cell types across the isocortex and hippocampal formation. Cell *184*, 3222–3241.e26. https://doi.org/10.1016/j.cell.2021.04.021.

40. Robel, S., Buckingham, S.C., Boni, J.L., Campbell, S.L., Danbolt, N.C., Riedemann, T., Sutor, B., and Sontheimer, H. (2015). Reactive astrogliosis causes the development of spontaneous seizures. J. Neurosci. *35*, 3330–3345. https://doi.org/10.1523/JNEUROSCI.1574-14.2015.

41. Gomez-Giro, G., Arias-Fuenzalida, J., Jarazo, J., Zeuschner, D., Ali, M., Possemis, N., Bolognin, S., Halder, R., Jager, C., Kuper, W.F.E., et al. (2019). Synapse alterations precede neuronal damage and storage pathology in a human cerebral organoid model of CLN3-juvenile neuronal ceroid lipofuscinosis. Acta Neuropathol. Commun. *7*, 222. https://doi.org/10.1186/s40478-019-0871-7.

42. Llavero Hurtado, M., Fuller, H.R., Wong, A.M.S., Eaton, S.L., Gillingwater, T.H., Pennetta, G., Cooper, J.D., and Wishart, T.M. (2017). Proteomic mapping of differentially vulnerable pre-synaptic populations identifies regulators of neuronal stability *in vivo*. Sci. Rep. *7*, 12412. https://doi.org/10.1038/s41598-017-12603-0.

43. Bourgeois, E.B., Johnson, B.N., McCoy, A.J., Trippa, L., Cohen, A.S., and Marsh, E.D. (2014). A toolbox for spatiotemporal analysis of voltage-sensitive dye imaging data in brain slices. PLoS One *9*, e108686. https://doi.org/10.1371/journal.pone.0108686.

YMTHE, Volume *30*

Supplemental Information

Neuronal genetic rescue normalizes brain network dynamics in a lysosomal storage disorder despite persistent storage accumulation

Rebecca C. Ahrens-Nicklas, Luis Tecedor, Arron F. Hall, Owen Kane, Richard J. Chung, Elena Lysenko, Eric D. Marsh, Colleen S. Stein, and Beverly L. Davidson

Supplemental Figure 1: Luciferase assay confirmation of expression from the 1665bp *Cln3* promoter. Luminescence was measured from plasmids expressing luciferase under control of the RSV promoter (red) and the *Cln3* 1665bp promoter (blue), as compared to an eGFP control.

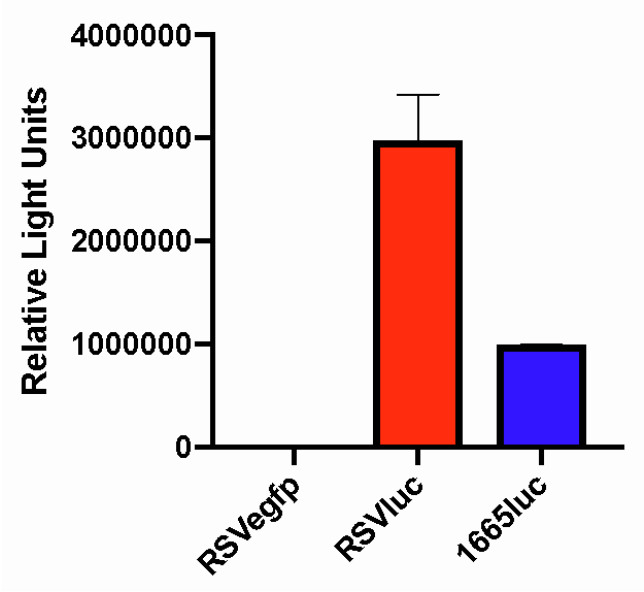

Supplementary Figure 2: AAV9-Cln3 and AAV9-GFP constructs

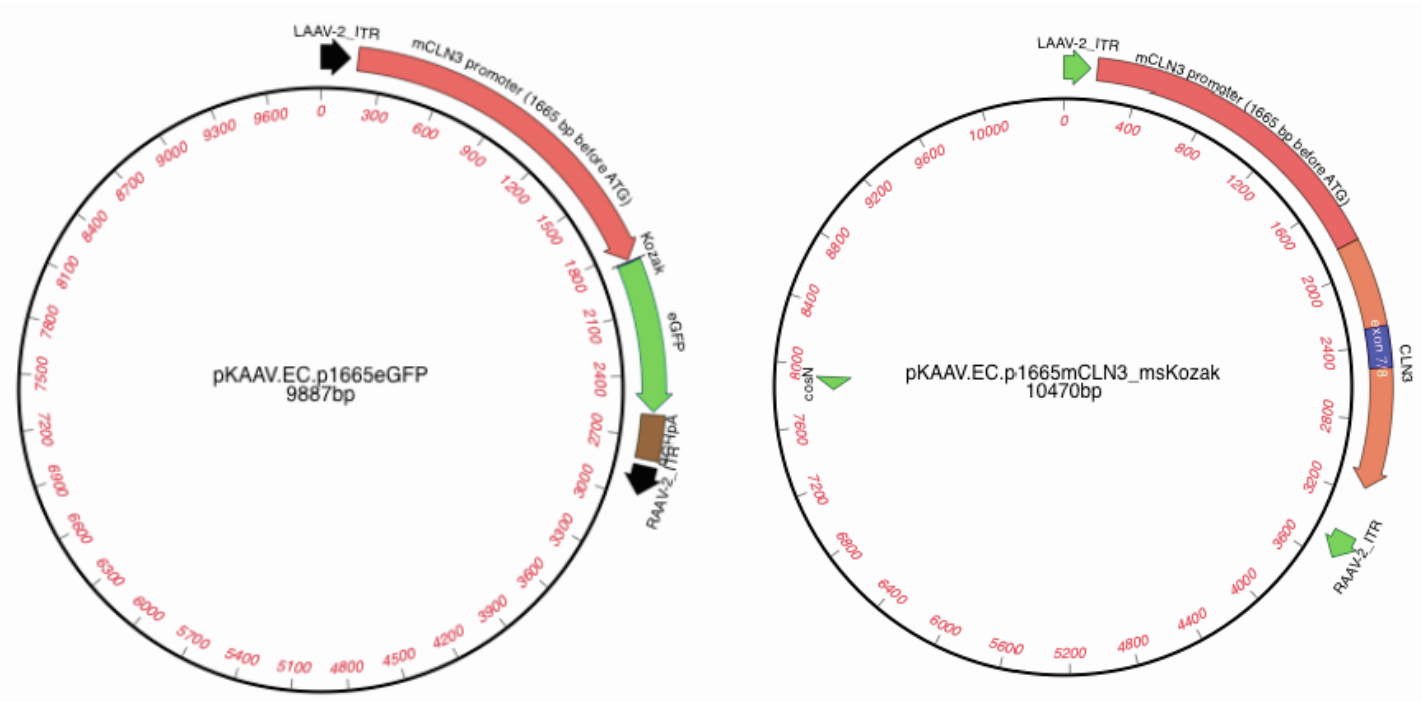

Supplemental Figure 3: p0 ICV injection of AAV9.1665GFP transduces both astrocytes and neurons. An AAV9 construct expressing GFP under the control of the 1665bp *Cln3* promoter was given via ICV injection into p0 wildtype pups. In 1-month-old mouse **(A)** cortex and **(B)** hippocampus, neurons, labeled with NeuN, were also GFP positive (examples shown by arrows). In addition, there were NeuN-negative, GFP positive astrocytes detected (examples shown by arrowheads). Sections from AAV.1665CLN3-treated animals that do not express GFP are shown as a negative control.

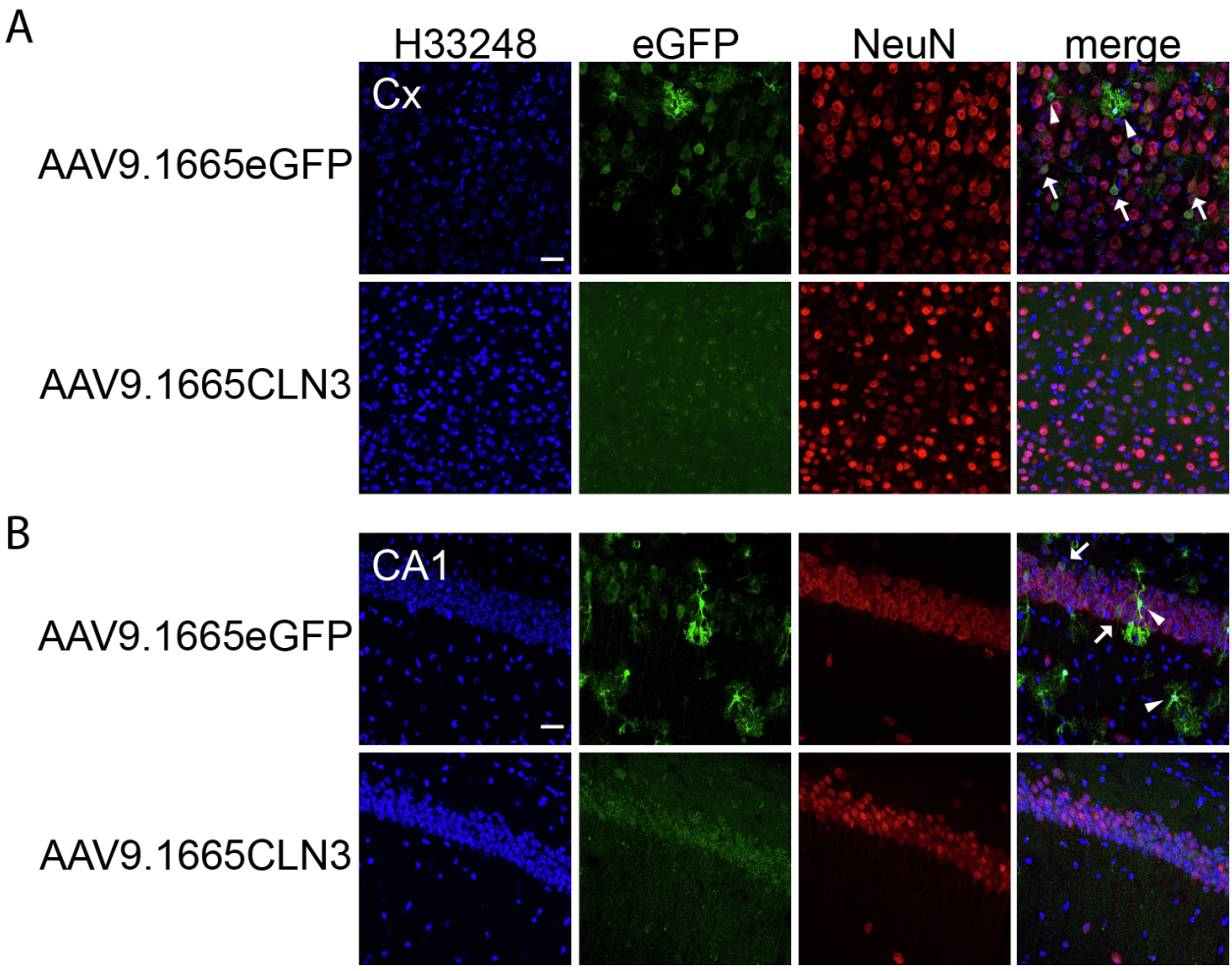

Supplemental Figure 4: p0 ICV AAV9-CLN3 injection prevents storage accumulation in the motor cortex of 12-month-old *Cln3*$^{\Delta ex78/\Delta ex78}$ mice. Staining for subunit C of the mitochondrial ATP synthase reveals lower levels of storage accumulation in AAV9.CLN3-treated *Cln3*$^{\Delta 78/\Delta 78}$ mice as compared to untreated controls. Genotypes compared using one-way ANOVA, followed by Tukey's multiple comparisons test, ****p<0.0001.

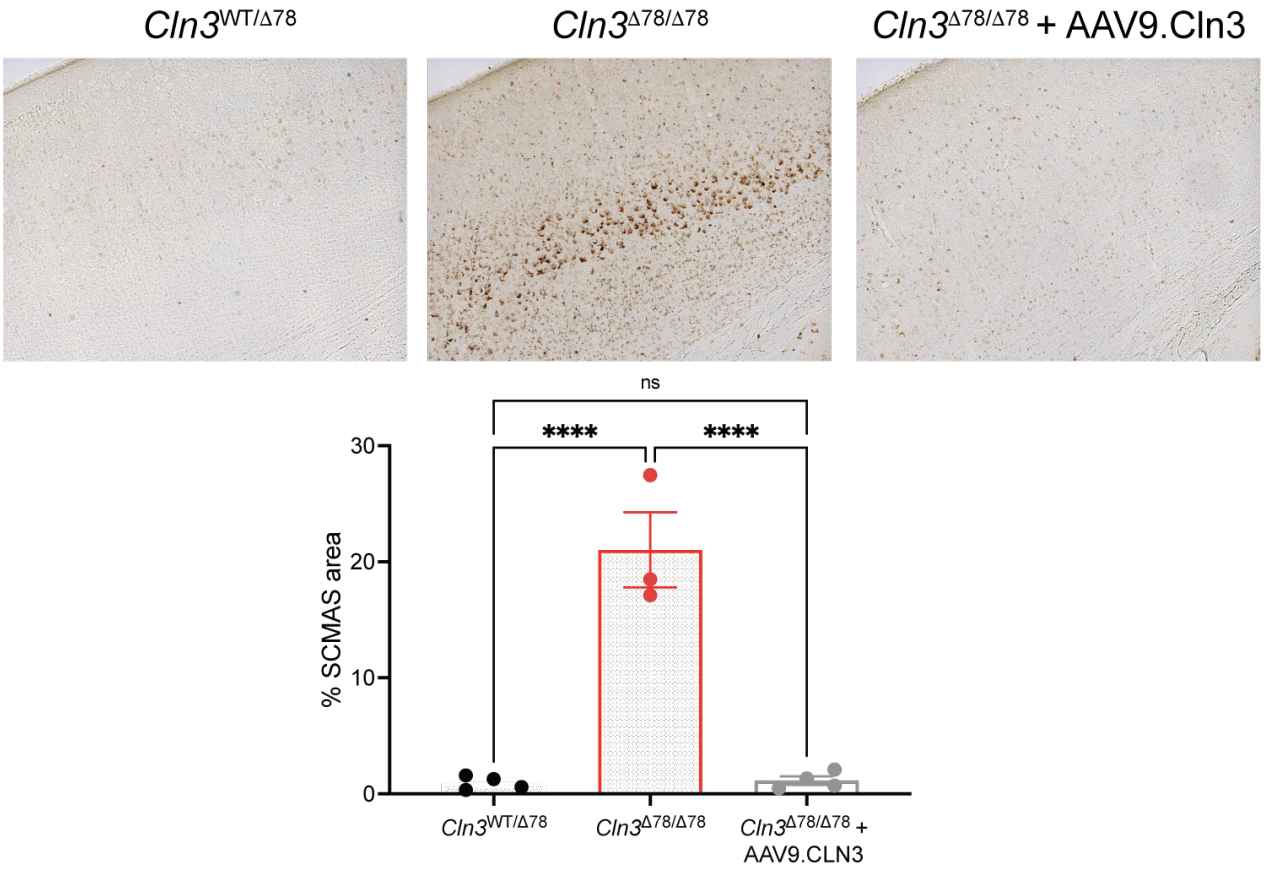

Supplemental Figure 5: Map of targeting vectors, pBT378-1665-FLEX-CLN3

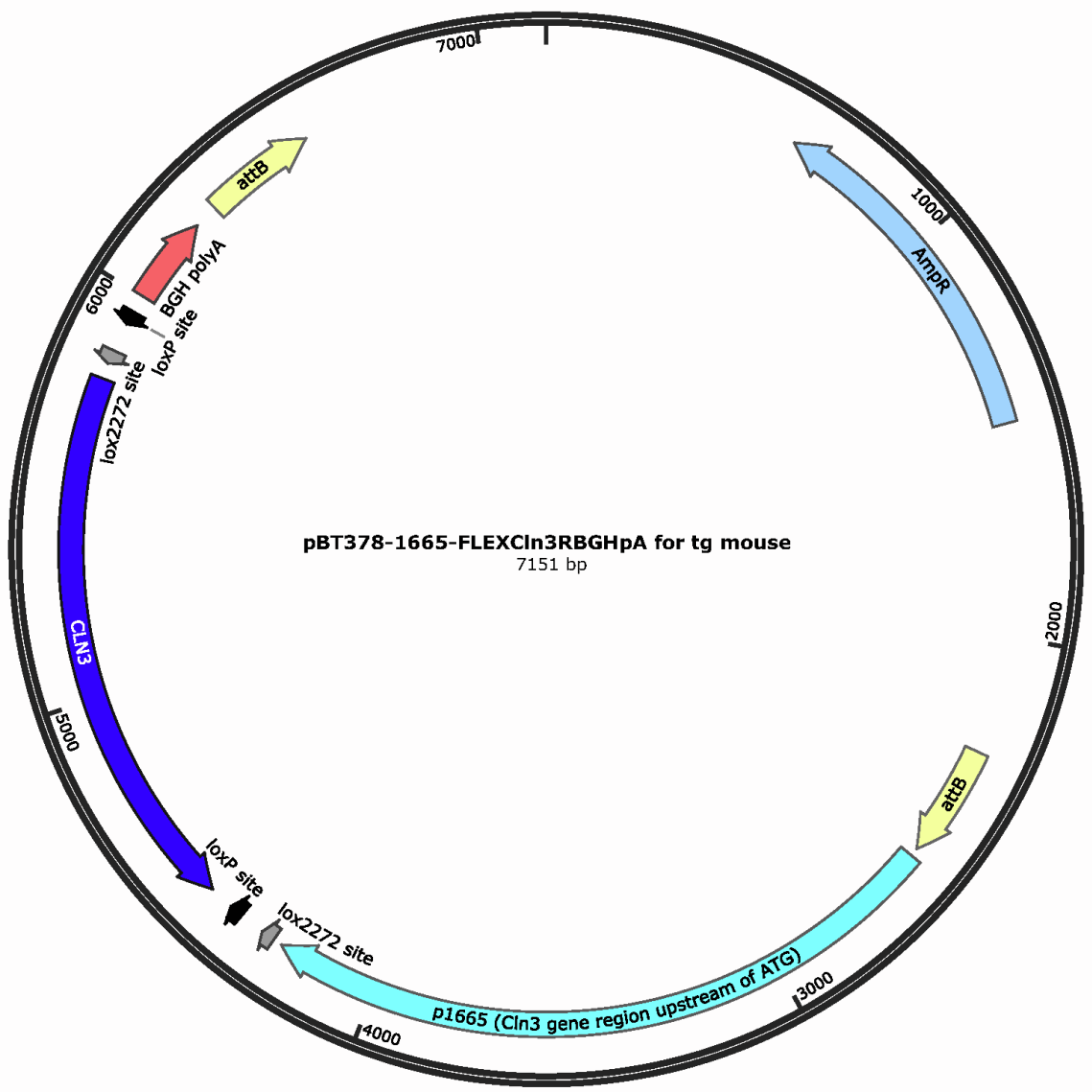

Supplemental Figure 6: Confirmation of Flex*Cln3* transgenic founders and first cross to *Cln3*$^{\Delta 78/\Delta 78}$ mice. **(A)** Schematic shows targeted H11P3 allele without and with transgene insertion. Insertion occurs at a pair of attP sites; insertion at attP1-2 is shown. PCR primers are indicated by arrows (forward in purple and reverse in green), and PCR reactions designated with blue lines. **(B)** Primer sequences and expected product sizes for PCR reactions. **(C)** PCR results from tail-snip DNA confirm transgene insertion for founder male 547#5 (at attP2-3) and for founder female 547#11 (at attP1-3). **(D)** PCR results from tail-snip DNA from litters of first cross of founders to Δex7/8. PCR4 indicates 5 of 29 pups have inherited the FLEXCln3R transgenic allele (417 bp band). Absence of transgene positive progeny from founder 547#5 indicates lack of germline transmission in this founder.

A

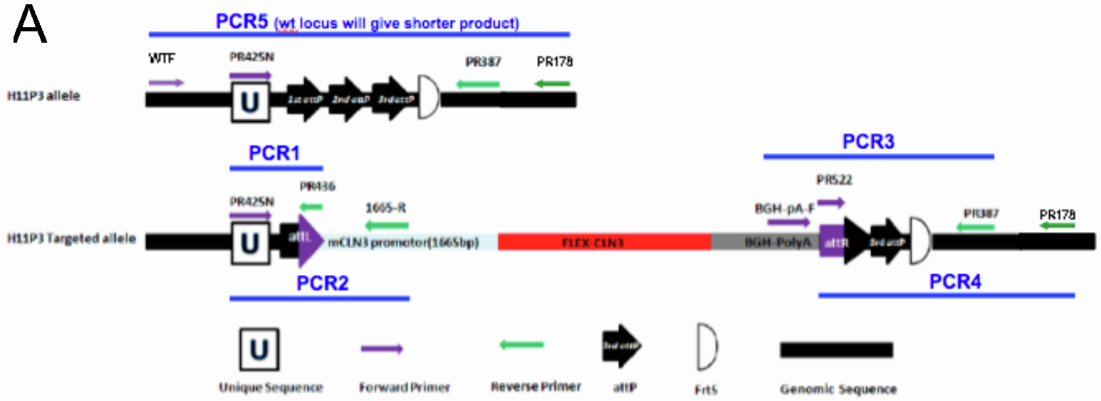

B

	insertion site	expected PCR product size
PCR1	attP 1-2	147 bp
	attP 1-3	147 bp
	attP 2-3	217 bp
PCR2	attP 1-2	425 bp
	attP 1-3	425 bp
	attP 2-3	495 bp
PCR3	attP 1-2	463 bp
	attP 1-3	393 bp
	attP 2-3	393 bp
PCR4	attP 1-2	487 bp
	attP 1-3	417 bp
	attP 2-3	417 bp
PCR5	no insertion	660 bp
	WT allele	323 bp

Primers for genotyping FLEXCln3 founders and progeny

PCRPR425N: 5'-GGTGATAGGTGGCAAGTGGTATTCCGTAAG -3'

PR436: 5'-ATCAACTACCGCCACCTCGAC -3'

1665-R: 5'-CAAACCCTAGCTTCCTCTCACTGAAG-3'

BGH-polyA-F: 5'-GCATCGCATTGTCTGAGTAGGTGTCA-3'

PR387: 5'-GTGGGACTGCTTTTTCCAGA-3'

PR522: 5'-CGATGTAGGTCACGGTCTCG -3'

PR178: 5'-TTCCCTTTCTGCTTCATCTTGC -3'

WTF: 5'-TGGAGGAGGACAAACTGGTCAC-3'

C

lane	mouse
1	547#5
2	547#11
3	WT mouse
4	no template control

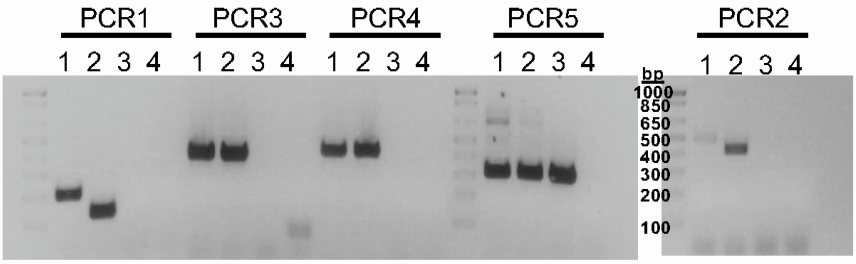

D

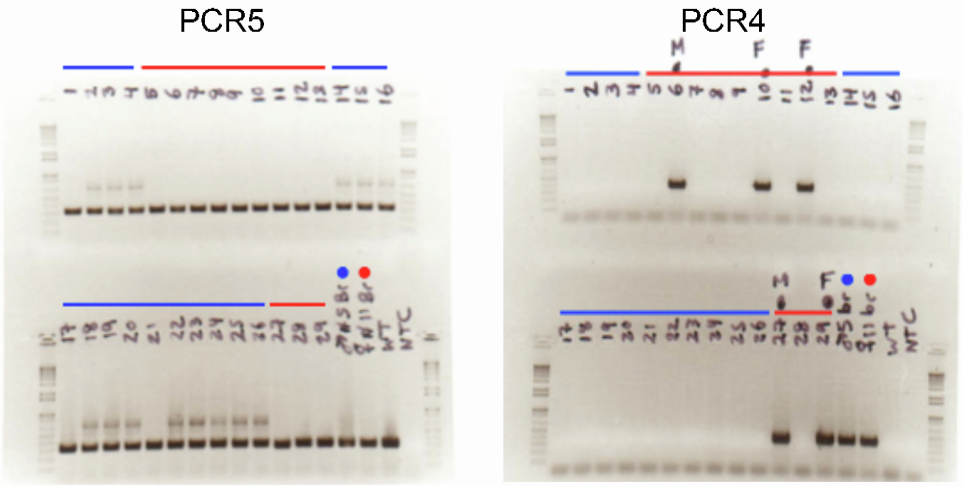

founder parent is 547#5 male

founder parent is 547#11 female

Supplemental Figure 7: Cre-mediated recombination of Flex*Cln3* allele in target tissues.
(TOP) Full uncut gels showing appropriately rearranged Flex*Cln3* transgene in genomic DNA extracted from hippocampus of *Zp3*-Cre+, *Gfap*-Cre+, and *Syn1*-Cre+ FlexCln3 animals. Lanes shown in Figures 2b and 3a are outlined and labeled. **(BOTTOM)** To confirm that the Flex*Cln3* allele rearranges appropriately in response to a number of Cre drivers, genomic DNA was extracted from the liver, spleen and brain of animals crossed to the drivers listed below. The Flex*Cln3* allele was detected to be in the forward orientation, indicating recombination occurred, in all tissue types in animals crossed to ubiquitous or endothelial Cre lines (lanes 1 and 2). When the Flex*Cln*3 animal was crossed to the neuronal Cre driver line, *Syn1*-Cre, (lane3) recombination only occurred in the brain. Lane 4 demonstrates that in the absence of Cre, the allele remains in the reverse orientation.

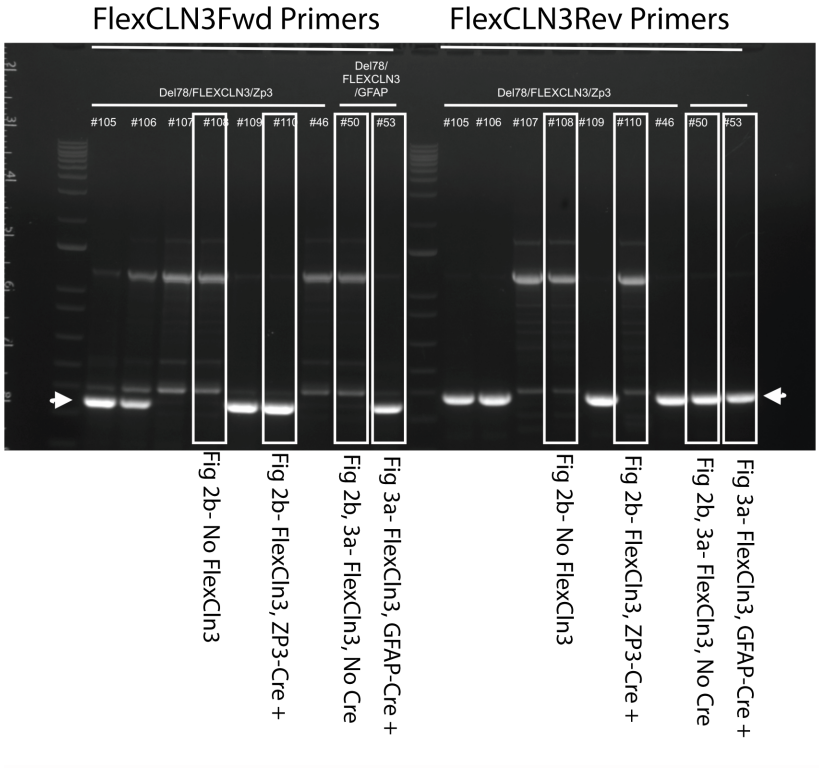

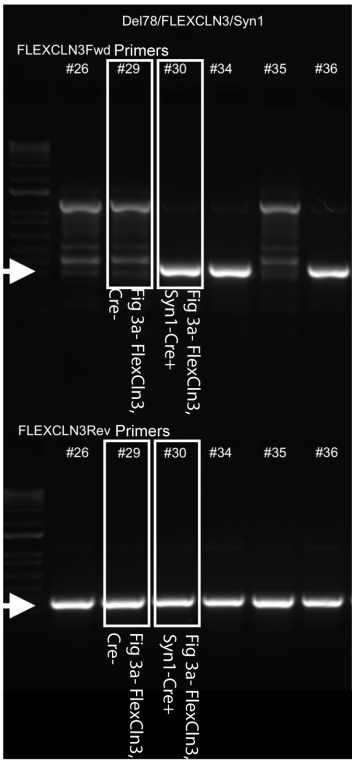

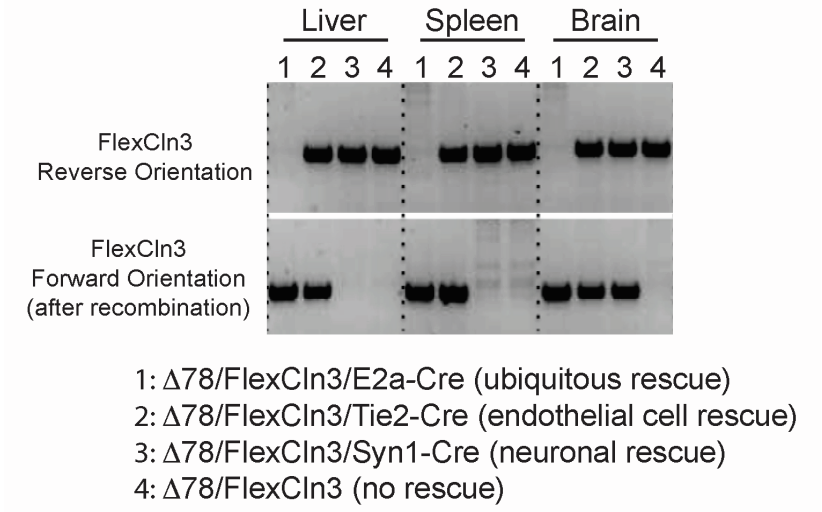

Supplemental Figure 8: Storage accumulation in Flex*Cln3* mouse. A. Western blot of NP40 detergent insoluble SCMAS and p62 protein in regional lysates from brain (N=4 per group). While SCMAS accumulation was improved in the ubiquitous rescue mouse, SCMAS still accumulated in the no rescue, endothelial cell rescue, and neuronal rescue conditions. We found no difference in p62 levels, a marker of autophagy induction in any condition. Therefore, we chose not to use this as a read-out of disease phenotype or response to rescue.

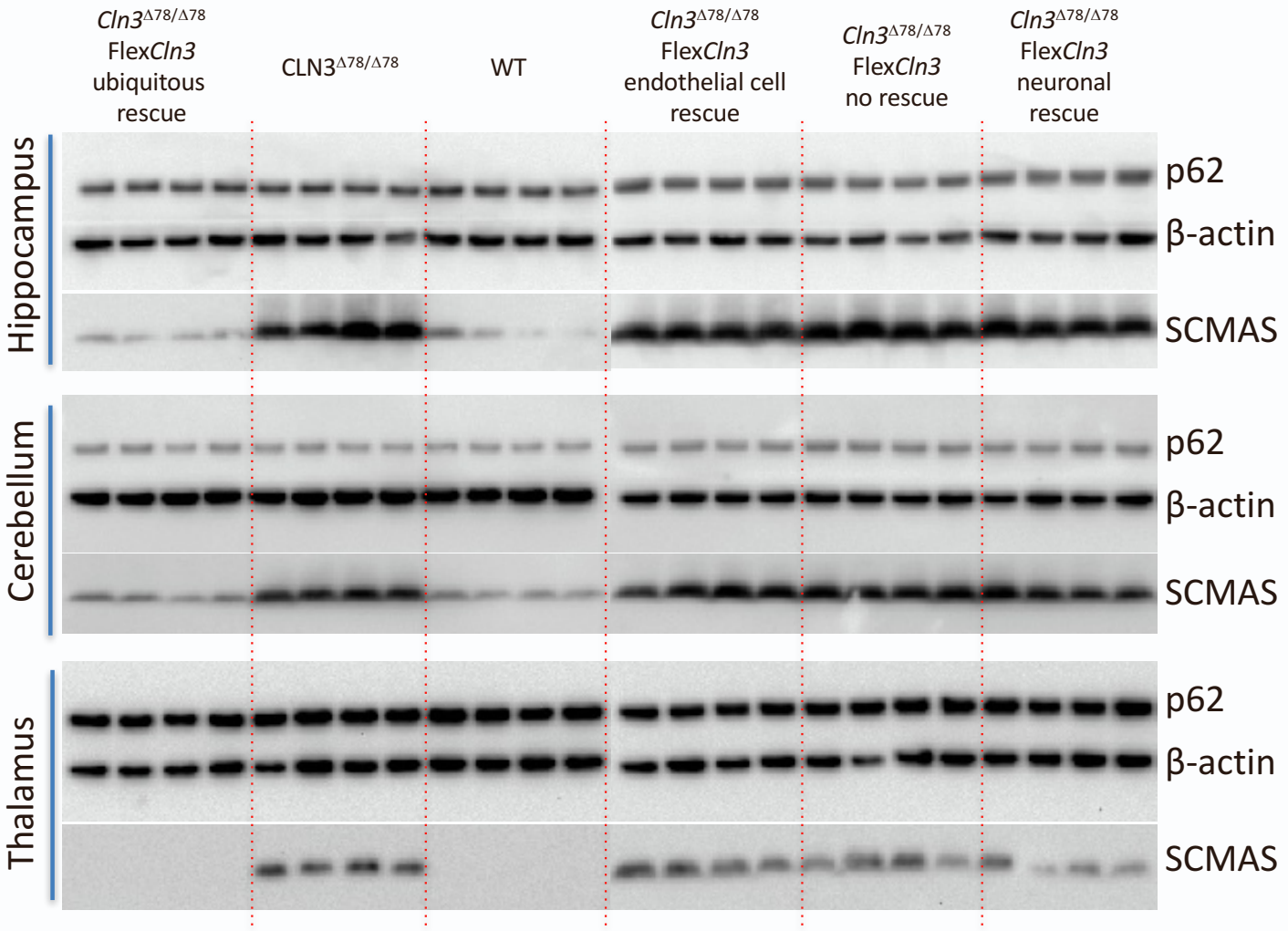

Supplemental Figure 9: Rescuing expression of *Cln3* in either astrocytes or neurons alone does not prevent storage accumulation in the hippocampus at 6 months of age. (A) 10X image of the CA3 region of six-month-old *Cln3*$^{WT/WT}$ hippocampus demonstrates little storage of subunit C of the mitochondrial ATP synthase (SCMAS) (green), as compared to **(B)** *Cln3*$^{\Delta ex78/\Delta ex78}$ hippocampus. **(C)** In Flex*Cln3* / *Cln3*$^{\Delta ex78/\Delta ex78}$ / *Gfap*-Cre animals, rescue of *Cln3* expression in astrocytes alone does not prevent SCMAS accumulation. **(D)** Expression of Flex*Cln3* in neurons alone (Flex*Cln3* / *Cln3*$^{\Delta ex78/\Delta ex78}$ / *Syn1*-Cre animals) also does not prevent storage accumulation.

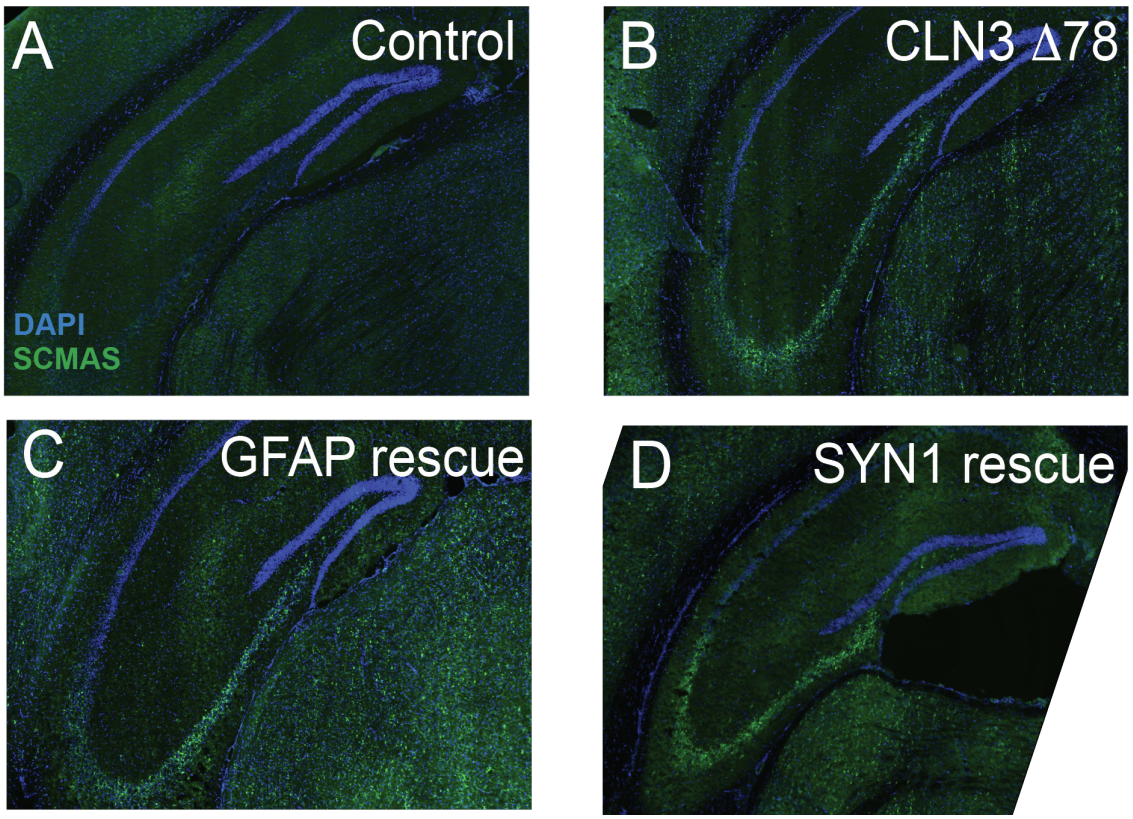

Supplementary Figure 10: Rescuing expression of *Cln3* in either astrocytes or neurons alone only partially improves astrocytosis in 12-month-old Flex*Cln3* mice. (A-B) 20X image of the CA3 region of $Cln3^{\Delta ex78/\Delta ex78}$ hippocampus demonstrates increased astrocytosis, as measured by GFAP staining as compared to $Cln3^{WT/WT}$ hippocampus. **(C-E)** Flex*Cln3* expression in astrocytes alone did not prevent astrocytosis in the CA3 region of the hippocampus. However, *Cln3* expression in neurons alone partially improves astrocytosis. **(F-G)** In the motor cortex, $Cln3^{\Delta ex78/\Delta ex78}$ mice demonstrate increased astrocytosis, as compared to $Cln3^{WT/WT}$ controls. **(H-J)** Flex*Cln3* expression in either astroctyes of neurons alone partially normalizes astrocytosis in the motor cortex. For both regions, n=4 animals, 6 images / animal, two-way ANOVA by animal and genotype, p<0.0001 for genotype, followed by Tukey's multiple comparisons test. For all panels: *p<0.05, **p<0.01, ***p<0.001, ****p<0.0001.

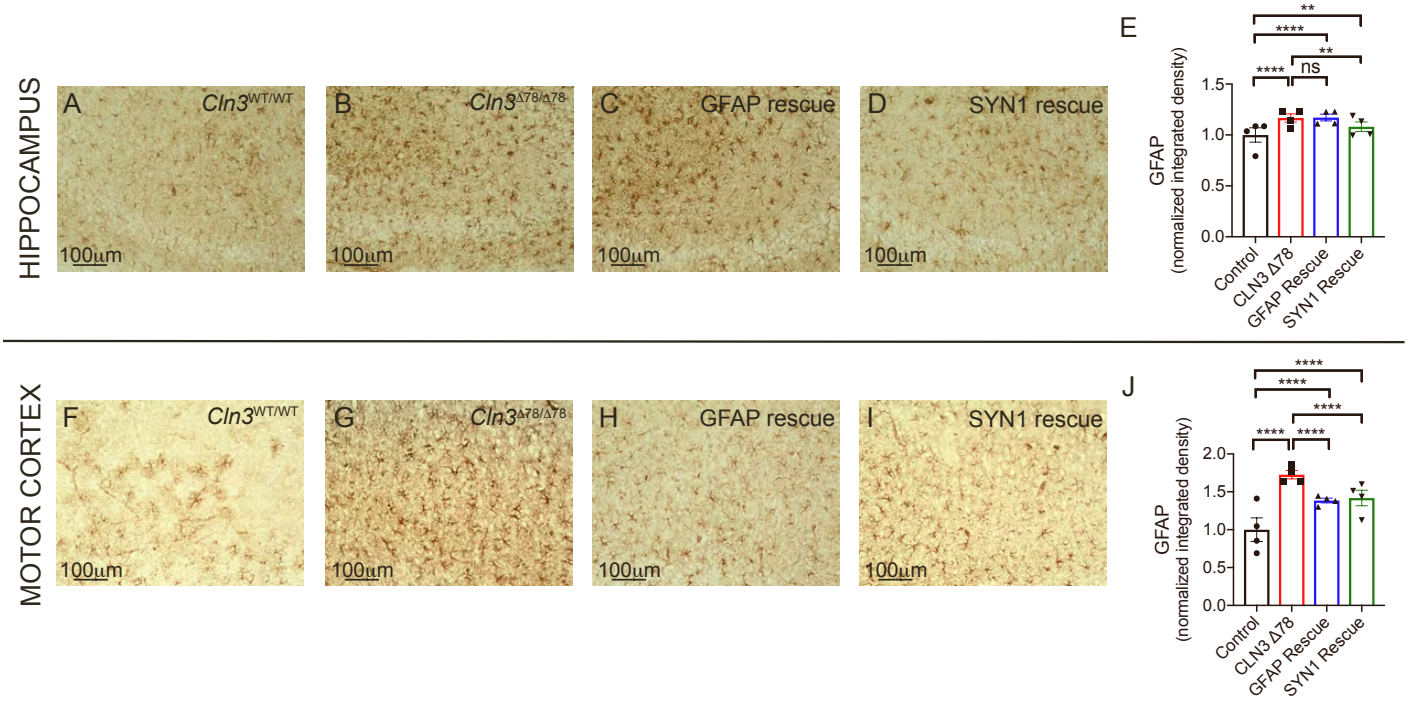

Supplemental Methods:

Luciferase assay for promoter validation

A luciferase assay was established to confirm expression from the 1665bp *Cln3* promoter **(Sup Figure 1)**. Specifically, 1665 bp from the murine Cln3 gene directly upstream of the translational start site (gene ID ENSMUSG00000030720.16; transcript ENSMUST00000032962.10, protein Uniprot Q61124) was obtained from C57BL6/J genomic DNA using PCR with:
Forward primer 5'-GAGGGGGCATTCGGCAAGTGCAGCC -3'
Reverse primer 5'-AACATTGAGTTCGGGTCCCCCAAAGGG-3'.

The p1665 sequence contains an osmotic response element (ORE) [1] at position 646-656 bp and a Coordinated Lysosomal Expression and Regulation (CLEAR) element for TFEB binding at position 1352-1361 bp[2]. The p1665 was initially cloned into pCRBlunt II-TOPO (Invitrogen) and from there was subcloned upstream of firefly luciferase in pGL2-basic vector (Promega) using restriction enzyme digest and standard cloning methods to create p1665luc. As a positive control, the RSV promoter was similarly cloned into pGL2-basic to create RSVluc.

MDCK cells (ATCC) were cultured in DMEM/F12 with 10% FBS. After trypsin harvest, cells were suspended in media at 100,000/ml and transfected with RSVluc or p1665luc plasmid via reverse transfection using Lipofectamine Ltx with Plus reagent (Invitrogen), at a ratio of 400ng plasmid/0.8 ul Lipofectamine Ltx/ 0.4ul Plus reagent/50,000 cells per well, in 24-well culture dishes. The media was changed the next day and three days post transfection cells were harvested into passive lysis buffer (Promega) containing 1x protease inhibitor (200ul lysis buffer per well) and lysates stored at -80°C till luciferase assay. Luciferase activity was determined using Promega luciferase kit reagents. Five microliters of lysate were assayed in duplicate in a luminometer plate reader, with readings collected after injection of 50 ul of substrate. Results are expressed as luminescence units (LU) ± standard deviation of duplicate cultures. To ensure results were within the linear range, lysate from RSVluc-transfected wells (1, 2, 5, 10, 20 ul) was assayed in duplicate on the same plate; all sample readings fell within the linear range.

AAV9-mediated gene replacement

Mouse *Cln3* and *eGFP* genes were PCR amplified from cDNA libraries and cloned into the pKAAV.EC.BGHpA backbone plasmid (**Sup Figure 2**). The CAG promoter in the backbone plasmid was substituted by 1665 bp sequence of the endogenous *Cln3* gene.

AAV9 viral vectors expressing *Cln3* or *eGFP* were generated using standard triple transfection methods and purification by CsCl gradient centrifugation [3]. Titers were quantified by silver stain after gel electrophoresis (SDS-PAGE) and qPCR.

Cryo-anesthetized neonatal pups (P0-P1) from $Cln3^{\Delta ex78/\Delta ex78}$ X $Cln3^{WT/\Delta ex78}$ breeders were ICV injected into the right lateral ventricle with 1E+10 vg AAV9 viral vectors in 2.5 µL according to published methods [4]. In brief, a 10 µL Hamilton microsyringe with a 33-gauge needle was used to penetrate the skull to a 2 mm depth at about 2.5 mm anterior to the lambda suture and 1 mm lateral to the sagittal suture. Injected mice were euthanized, and brain tissue analyzed 1 month or 1 year after injection. We confirmed transduction of both neruons and astrocytes in 1 month old mice after treatment with the AAV9.1665eGFP vector (**Sup Figure 3**). At 12 months of age, gene replacement in $Cln3^{\Delta ex78/\Delta ex78}$ lead to a partial reduction of storage accumulation in the cortex (**Sup Figure 4**).

FlexCln3 mouse generation

The Flex*Cln3* mouse was generated using previously-published TARGATT technology (Applied StemCell, ASC) [2]. Specifically, a plasmid containing the Flex*Cln3* allele with 1665bp of the endogenous Cln3 promoter was created (**Sup Figure 5**). The targeting construct contained the following features flanked by attB sites: p1665-lox2272(for)-loxP(for)-Cln3 cDNA(rev)-lox2272(rev)-loxP(rev)-BGH polyA. Once transgenic mice are established and bred to cre recombinase driver strains, the lox2277/loxP sequences allow for cre-recombinase mediated flip/excision steps, to place the Cln3 cDNA into forward orientation, triggering expression driven by the p1665 promoter. The targeting construct was used by ASC for microinjection into C57BL6 zygotes for attB-dependent recombination into attP receptor sites in the H11 gene locus.

Successful integration in four founder animals was identified by PCR using a panel of primers **(Sup Figure 6)**. Identification of appropriate founders included validation using 4 different PCR primer pairs:

PCR 1: PR425N/PR436. PR425N (forward primer) binds to the unique sequence on H11P3 allele, PR436 binds to partial sequence of attL. P425N/PR436 pair is to detect site-specific integration at 5' integration site. Expected PCR fragment is 217bp for 2, 3 insertion or 147bp for 1, 2 or 1, 3 insertion.

PCR 2: PR425N/1665-R. PR425N binds to the unique sequence on H11P3 allele, while 1665-R (reverse primer) recognizes the sequence within 1665 promoter region. A combination of PR425N and 1665-R can

be used to amplify 5' novel junction upon the successful integration of transgene. Anticipated DNA amplification fragment is 495 for 2, 3 insertion, or 425bp for 1, 2 or 1, 3 insertion.

PCR 3: BGH-pA-F/PR387: BGH-pA-F binds to BGH polyA sequence, while PR387 (reverse primer) binds to H11 genomic sequence downstream of 3' junction. The PCR amplification using BGH-pA-F/PR387 pair produces a 393bp (1, 3 or 2, 3 insertion) or 463bp (1, 2 insertion) fragment with part of BGH-polyA and partial H11 genomic sequence.

PCR 4: PR522/SH178. PR522 binds to partial sequence of attR. PR178 binds to a region in H11P3 locus downstream of the integration site. PCR amplification using PR522/PR178 pair is to detect site-specific integration at 3' integration site. Expected PCR fragment is 417bp for 2, 3 or 1, 3 insertion, or 487bp for 1, 2 insertion.

Generation of cell-type specific rescue models

Founder Flex*Cln3* mice were confirmed by PCR and one founder was selected to maintain the transgenic line **(Sup. Figure 6**). The transgenic line, mice harboring the Flex*Cln3* allele, as well as the Cre recombinase driver strains used in this study, were crossed to the well-established $Cln3^{\Delta ex78}$ mouse model[5] (Jackson Labs, B6.129(Cg)-$Cln3^{tm1.1Mem}$/J, Strain #017895). This model harbors the most common human CLN3 disease mutation, and manifests histopathologic features of CLN3 disease including progressive storage accumulation. For these experiments, 3 Flex*Cln3* lines were generated: 1) To express the Flex*Cln3* in all cell types (ubiquitous rescue), Flex*Cln3* / $Cln3^{\Delta ex78/\Delta ex78}$ were crossed to mice expressing Cre recombinase under the control of the E2a (B6.FVB-Tg(EIIa-cre)C5379Lmgd/J, Strain # 003724) or *Zp3* promoter [6] (*Zp3*-Cre, Jackson Labs, B6.Cg-Tg(Zp3-cre)1Gwh/J, Strain #06888) for recombination at germline level 2) To selectively express the wild-type Flex*Cln3* transgene in neurons, Flex*Cln3* / $Cln3^{\Delta ex78/\Delta ex78}$ mice were crossed to previously described mice expressing Cre recombinase under control of the Synapsin-1 promoter[7] (*Syn1*-Cre, Jackson Labs, B6.Cg-Tg(Syn1-cre)671Jxm/J, Strain #003966). 3) To express wild-type Flex*Cln3* in astrocytes, Flex*Cln3* / $Cln3^{\Delta ex78/\Delta ex78}$ mice were crossed to previously described mice expressing Cre recombinase under control of the glial fibrillary acidic protein promoter[8] (*Gfap*-Cre, Jackson Labs, B6.Cg-Tg(Gfap-cre)77.6Mvs/2J, Strain #024098). This particular *Gfap-Cre* line was used, as opposed to strain Jackson Labs, FVB-Tg(GFAP-cre)25Mes/J, Strain #004600, which also has expression in some neuronal and microglia populations in addition to astrocytes and neuronal progenitors.

Verification of Cre-mediated transgene flipping in genomic DNA from target tissues

For each line, tissue-specific Cre-mediated recombination of the Flex*Cln3* allele was confirmed through PCR of genomic DNA extracted from liver, spleen and brain **(Fig 2, 3 and Sup. Figure 7)**. For initial confirmation of Flex*Cln3* allele recombination and flipping in target tissues, genomic DNA was extracted from Flex*Cln3* / $Cln3^{\Delta ex78/\Delta ex78}$ mice crossed to the Cre-driver lines above.

For confirmation of orientation of the Flex*Cln3* allele via PCR of genomic DNA from target tissues the following primers were used:

Reverse orientation of the Flex*Cln3* transgene:

Forward primer: 5'-TGGGGCTCTGAGTCGGTCTC-3'

Reverse primer: 5'-TGGGAGTGGCACCTTCCAGG-3'

Product size 380 bp.

Forward orientation of the Flex*Cln3* transgene

Forward primer: 5'-GGAGACCAGTGACAAGCACCG-3'

Reverse primer: 5'-TGGGAGTGGCACCTTCCAGG-3'

Product size 345 bp.

Expression of FlexCln3 transcripts

Cln3 expression was quantified from the whole hippocampus of 4-month-old mice. Samples were flash-frozen in 200 µL of TRIzol reagent (Invitrogen, ThermoFisher Scientific) per sample. RNA was isolated in 1mL TRIzol followed by DNase treatment with TURBO DNA-free kit (Invitrogen, ThermoFisher Scientific), according to manufacturer's protocols. RNA concentration was calculated and purity tested for 260/280 ratio greater than 1.9 by NanoDrop 2000 (ThermoFisher Scientific). cDNA was synthetized from 2 µg RNA by reverse transcription using Superscript III or High capacity cDNA reverse transcription kit (Life Technologies, Carlsbad, CA) with RT random primers according to the manufacturer's recommendations. Quantitative PCR reactions were performed on a CFX384 Real Time System (Bio-Rad, Hercules, CA). A custom PrimeTime primer/probe assay (IDT-integrated DNA Technologies (Coralridge, IA) was used for amplification of forward-oriented FLEX*Cln3* transcripts off the transgenic allele:

Forward primer: 5'-GCTCGAGCATGCATCTAGTATAA-3'

Reverse primer: 5'-AAGGCACAGTCGAGGTCTA-3'

Probe: 56-FAM/AGGTTCGAA/ZEN/TTCGATATCGCGGCC/3IABkFQ

A commercially available primer/probe assay for murine *Cln3* (IDT assay Mm.PT.58.9756823) recognizing wildtype (exon 7/8-containing) transcripts was used to amplify *Cln3* transcripts from control mice (*Cln3*$^{\Delta ex78/WT}$or *Cln3*$^{WT/WT}$) and from the FLEX*Cln3* locus of ubiquitously rescued mice. *ACTB* (control mix-VIC, Applied Biosystems, #4351315) was used as a reference gene to normalize *Cln3* expression levels by the delta delta cycle threshold (ddCt) method.

Western Blot for subunit C of the mitochondrial ATP synthase (SCMAS)

Mice were euthanized under anesthesia, the brain removed and regions isolated by dissection in ice-cold PBS under a dissecting microscope, and snap frozen in liquid nitrogen. Samples were stored at -80°C until processing. Tissues were processed by homogenization in Eppendorf microcentrifuge tubes in ice-cold lysis buffer (50 mM Tris pH 7.5, 150 mM NaCl, 1% NP40, 0.1% SDS, 0.5% DOC, with 1x Roche protease inhibitors). After 20 min incubation on ice, lysates were centrifuged at 1600xg for 5 min at 4 °C to pellet debris, and lysates transferred to fresh tubes. Protein concentrations were determined (BioRad DC assay) and concentrations equilibrated to 2 mg/ml, and 450 ul of each lysate was centrifuged at 20,817xg for 30 min at 4 °C. Supernatants (detergent-soluble fraction) were transferred to fresh tubes. Pellets (detergent-insoluble fraction) were dispersed in 500 ul lysis buffer and the centrifugation step repeated. Washed pellets were resuspended in 90 ul lysis buffer supplemented with 1% SDS and 1x NuPage and sonicated for 3 s on ice. NuPage loading buffer was added to the detergent-soluble samples.

All samples were heated at 70 °C for 10 min and 16 ul/lane loaded onto precast NuPage 4-12% Bis-tris mini-gels, with Spectra Multicolor Broad Range protein ladder (Thermofisher), run in MES buffer, and transferred overnight in a Mini Trans-Blot Cell (BioRad) in Tris-glycine transfer buffer containing 10 % methanol and 0.01% SDS at 4 °C with constant 30 V onto PVDF membranes. Membranes were blocked by 1 h incubation in 5% dried milk powder in PBS with 0.05% tween (PBST), then cut into strips for overnight incubation at 4 °C with primary antibody diluted in 2.5% dried milk in PBST. Antibodies to the following antigens were used for blotting: SCMAS at 1/3000 (polyclonal rabbit antisera from Elizabeth Neufeld); p62 at 1/4000 (Abnova #H00008878-MO1 mouse IgG clone 2C11, 0.5 mg/ml stock); beta-actin at 1/20,000 (Sigma mouse IgG clone AC-15 ascites). After primary antibody incubation, blots were washed in PBST and incubated with HRP-conjugated secondary goat-anti-rabbit IgG or goat-anti-mouse IgG (Jackson ImmunoResearch) for 1 h at RT. Blots washed and developed with ECL prime (Amersham) and chemiluminescent images captured and analyzed using a Versadoc image capture system with Quantity One software (Bio-Rad). Beta-actin was used as a loading control, and band

densities for SCMAS and p62 were normalized to beta-actin in each lane. Graphs show the relative mean band intensity ± standard deviation between groups.

Histology

Immunohistochemical analysis of fixed brains was carried out as previously described[9]. Mice were anesthetized with isoflurane and transcardially perfused with saline and 4% paraformaldehyde (PFA) in 0.1 M phosphate buffer (MilliporeSigma), pH 7.4. The brains were then postfixed in 4%PFA at 4°C overnight, cryoprotected with 30% sucrose buffer and embedded in OCT. Coronal sections (20 μm) were cut using a cryostat (Microm HM 500) and stored at –80°C until staining.

For mitochondrial ATP synthase subunit C (SCMAS) staining, sections were washed with PBS, permeabilized with 0.1% Triton X-100 in PBS for 7 minutes, washed again with PBS 3 times, and blocked in 3% bovine serum albumin, 5% goat serum, 0.2% Triton X-100 in PBS for 1 hour, all at room temperature. Sections were incubated with a primary antibody against subunit C of the mitochondrial ATP synthase (SCMAS) (Abcam 181243, 1:500).

For GFAP staining, sections were washed with PBS, permeabilized with 0.1% Triton X-100 in PBS for 7 minutes, incubated in 3% H2O2/10% methanol in PBS for 5 minutes, washed again with PBS 3 times, and blocked in 10% normal goat serum with 0.1% Triton X-100 in PBS for 1 hour, all at room temperature. Sections were incubated with a primary antibody against GFAP (Dako Z0334, 1:1000) at 4°C overnight.

For NeuN staining, sections were washed with PBS, permeabilized with 0.1% Triton X-100 in PBS for 7 minutes, incubated in 3% H2O2/10% methanol in PBS for 5 minutes, washed again with PBS 3 times, and blocked in 10% normal goat serum in PBS, all at room temperature. Sections were incubated with an antibody against NeuN (MilliporeSigma MAB377, 1:100) at 4°C overnight.

To detect the primary antibody using DAB staining, sections were incubated with a biotinylated secondary antibody (Jackson ImmunoResearch, 1:500) at room temperature for 30 minutes, followed by PBS washes and incubation in avidin-biotin complex (Vectastain, Vector Laboratories) at room temperature for 1 hour. Slices were incubated in DAB solution for visualization.

To detect the primary antibody using immunofluorescence, sections were incubated with a FITC-conjugated secondary antibody (Jackson ImmunoResearch, 1:50) at room temperature for 30 minutes,

followed by PBS washes. For immunofluorescence, all auto-fluorescence was quenched by incubation for 30 seconds in TrueBlack (Biotium, 50ul of 20X stock in 1ml of 70% ethanol).

All images were acquired on a Keyence BZ-X800 or a Leica DM600B microscope and analyzed in a blinded fashion. At least 4 animals per genotype were analyzed. For quantification of SCMAS staining in the genetic rescue mice, Keyence BZ-X800 analysis software was used to calculate the percent area of fluorescence. In the CA3 region, one 10X image of the entire hippocampal CA3 region was captured per animal, while in the motor cortex at least 4, 20X images/animal were acquired. For GFAP staining, at least 4, 20X images / animal were acquired for both the motor cortex and CA3 regions. Images were converted to 8-bit grayscale images and the integrated density of the image was calculated in ImageJ, using rolling ball radius background subtraction.

For quantification SCMAS in the AAV-rescue experiments, five different 152x152 pixel regions of the hippocampus were quantified and averaged in each of 3-4 animals. Color images were transformed to black and white 8-bit format, thresholded for immunopositive signal and the percent area was quantified.

For colocalization of autofluorescence and NeuN staining, 3 mice per group were analyzed with 3 images per mouse. Each image was fragmented for NeuN immunostaining, and autofluorescence was quantified in 238 or more NeuN-positive cells per group using FIJI software. Data represents mean gray value for each cell.

Voltage Sensitive Dye Imaging

In vitro voltage sensitive dye imaging (VSDI) of hippocampal slices was completed as previously described[9]. 400µm hippocampal-entorhinal cortical (HEC) slices, which preserve the hippocampal trisynaptic circuit [10-14], were prepared as per our standard protocols[15]. High-sucrose cutting solution contained in mM, 192 sucrose, 2.5 KCl, 1.25 NaH_2PO_4, 26 $NaHCO_3$, 12.2 glucose, 3 sodium pyruvate, 5 sodium ascorbate, 2 thiourea, 10 $MgSO_4$, 0.5 $CaCl_2$. After cutting, slices recovered for 45 min at 37°C and 45 min at room temperature prior to recordings in an artificial cerebrospinal fluid (ACSF) containing, in mM, 115 NaCl, 2.5 KCl, 1.4 NaH_2PO_4, 24 $NaHCO_3$, 12.5 glucose, 3 sodium pyruvate, 5 sodium ascorbate, 2 thiourea, 1 $MgSO_4$, 2.5 $CaCl_2$. For recording, slices remained in a standard ACSF solution containing, in mM, 128 NaCl, 2.5 KCl, 1.4 NaH_2PO_4, 26.2 $NaHCO_3$, 12.2 glucose, 1 $MgSO_4$, 2.5 $CaCl_2$.

The VSD di-3-ANEPPDHQ (Invitrogen) was solubilized in 95% ethanol (0.020 mg/uL) and stored at -

20°C. Slices were stained with the di-3-ANEPPDHQ (0.1 mg/mL, in ACSF) for 14-16 minutes and transferred to a humidified interface chamber (BSC2, Scientific Systems Design), for recording. Excitation light was provided by 7 high-power green LEDs (Luxeon Rebel LXML-PM01-0100, Philips) coupled to a 535 ± 25 nm filter and 565 nm dichroic mirror. A 610 nm longpass filter further isolated the emitted fluorescence. Fluorescence was recorded at 1000 frames per second with a fast video camera with 80 x 80 pixel resolution (NeuroCCD, Redshirt Imaging, Decatur, GA).

For experiments, four 0.1ms pulses at 10Hz were delivered via a bipolar tungsten electrode (model ME12206, World Precision Instruments) positioned to stimulate the perforant pathway.
Stimulus strength was set at the current required to produce a saturating field potential response in the granule cell layer of the dentate gyrus using a glass electrode pulled to a 2-8 MΩ tip, and filled with ACSF. All recordings were 1.5 s long, with a 10 s delay between recordings to allow fluorescence to recover from photobleaching. Thirteen recordings of evoked activity were interleaved with 13 VSDI runs where no stimulus was delivered. Runs without delivered stimuli were used for offline subtraction to correct for any baseline drift over the course of a recording.

Post-collection VSDI analysis was completed using the previously published VSDI toolbox [15], which allows for robust statistical analysis across both spatial and temporal dimensions. The algorithm creates unbiased regions of interest over the entire dentate gyrus, and the fluorescence response in each ROI for each image is calculated. As previously published [15], in order to compare between and average slices linear interpolation was used in order to "stretch" rasters to be the same size. For all studies, a final stretched DG raster size was 22 ROIs, including 11 covering the internal and external blades each.

A two-dimensional raster plot showing the location, time and fluorescence change for each slice was generated. In addition to individual rasters for each slice, an average raster plot per condition was generated. The raster plots from different genotypes were compared using a permutation sampling method with n=1000 permutations. A heatmap showing regions of the network with statistically significant (p<0.05) differences was created. Group sizes for VSD studies were as follows: *Cln3*$^{\Delta ex78/WT}$ 23 slices from 4 animals; *Cln3*$^{\Delta ex78/\Delta ex78}$ 30 slices from 6 animals; Flex*Cln3* / *Cln3*$^{\Delta ex78/\Delta ex78}$ / *Gfap*-Cre 19 slices from 4 animals; Flex*Cln3* / *Cln3*$^{\Delta ex78/\Delta ex78}$ / *Syn1*-Cre 17 slices from 4 animals.

EEG acquisition and analysis

EEG recording electrodes were constructed and implanted as previously described [9]. Specifically, recording headcaps were created by attaching 1 ground, 1 reference, and 6 cortical leads lead (0.004

inches, formvar-coated silver, California Fine Wire), and 2 hippocampal leads (0.005 inches bare, 0.008 inches coated, stainless steel wire, AM-Systems) to a microconnector (Omnetics). For implantation, mice were premedicated with intramuscular ketamine/xylazine followed by inhaled isoflurane anesthesia. The following stereotaxic coordinates (measurements relative to bregma) were used to implant electrodes: bilateral motor cortices: 0.5 mm rostral, 1 mm lateral, and 0.6 mm deep; bilateral barrel field cortices: 0.7 mm caudal, 3 mm lateral, and 0.6 mm deep; bilateral visual cortex: 3.5 mm caudal, 2 mm lateral, and 0.6 mm deep; and bilateral hippocampus (CA1 region): 2.2 mm caudal, 2 mm lateral, and 1.7 mm deep. The cerebellar reference lead was implanted posterior to lambda. The ground wire was wrapped tightly around a 1/8-inch self-tap screw (Precision Screws and Parts), which was inserted into the skull rostral to the motor cortex leads. To aid in securing the recording cap, a second screw was inserted caudal to lambda. The recording electrodes were secured with dental cement. The animal was allowed to recover for at least 18 hours before recording. Each mouse was connected to a RHD2000 low-noise amplifier chip (Intan Technologies), and connected to a data acquisition board by a lightweight cable. Electrophysiologic data was acquired at 2 kHz using the Intan RHD2000 Recording system software (http://intantech.com/downloads.html). 12-15 month old animals from each genotype group (n=4-5 animals/group) were recorded for at least 24 hours.

All EEG analysis was completed in MATLAB as previously described[9].

EEG Analysis

EEG was analyzed as previously described [9]. Steps included:

1) Detection of poor-quality recording channels: An automated artifact detector was used on each recording channel for each 30-minute recording period before analysis. Detection of a noisy or poorly recording channel was completed by calculating the average of the root mean squared amplitude and skew of the voltage for each second of the recording. Channels with a root mean square amplitude of less than 30 μV or more than 200 μV or a skew greater than 0.4 were excluded from further analysis.

2) Spike detection: A spike detector algorithm designed to detect voltage deflections that were greater than 5 standard deviations above the mean with a full width at half maximum amplitude of 5–200 ms was used to detect spikes. Spikes were eliminated if they occurred within 10-seconds of a deflection found to be an artifact (i.e., it had a half width outside the 5- to 200-ms range). Multi-channel spikes were defined as a spike occurring in at least 2 of 8 EEG channels.

3) Power analysis: To analyze mutation-induced discrepancy in background EEG frequency composition, recordings were divided into 5-second epochs for power analysis. Epochs containing large amplitude artifacts, most likely due to movement (defined as a peak *Z*-score of the root mean squared voltage amplitude greater than 3), were excluded from frequency analysis. Fast Fourier transform analysis was then completed on artifact-free epochs. Quantification of the power in each of the major EEG frequency bands (delta 0.1–4.0 Hz, theta 4–8 Hz, alpha 8–13 Hz, beta 13–25 Hz, and gamma 25–50 Hz) was completed. Power in each band across all epochs was averaged and power in each band was normalized to total power.

Supplementary References:

1. Ferraris, J. D. & Garcia-Perez, A. Osmotically responisve genes: The mammalian osmotic responsive element (ORE). *American Zoology* **41,** 734–742 (2001).
2. Palmieri, M. *et al.* Characterization of the CLEAR network reveals an integrated control of cellular clearance pathways. *Hum. Mol. Genet.* **20,** 3852–3866 (2011).
3. Ayuso, E. *et al.* High AAV vector purity results in serotype- and tissue-independent enhancement of transduction efficiency. *Gene Ther* **17,** 503–510 (2010).
4. Hua, Y. & Krainer, A. R. Antisense-mediated exon inclusion. *Methods Mol. Biol.* **867,** 307–323 (2012).
5. Cotman, S. L. *et al.* Cln3(Deltaex7/8) knock-in mice with the common JNCL mutation exhibit progressive neurologic disease that begins before birth. *Hum. Mol. Genet.* **11,** 2709–2721 (2002).
6. Shafi, R. *et al.* The O-GlcNAc transferase gene resides on the X chromosome and is essential for embryonic stem cell viability and mouse ontogeny. *Proc Natl Acad Sci USA* **97,** 5735–5739 (2000).
7. Zhu, Y. *et al.* Ablation of NF1 function in neurons induces abnormal development of cerebral cortex and reactive gliosis in the brain. *Genes Dev.* **15,** 859–876 (2001).
8. Gregorian, C. *et al.* Pten deletion in adult neural stem/progenitor cells enhances constitutive neurogenesis. *J. Neurosci.* **29,** 1874–1886 (2009).
9. Ahrens-Nicklas, R. C. *et al.* Neuronal network dysfunction precedes storage and neurodegeneration in a lysosomal storage disorder. *JCI Insight* (2019). doi:10.1172/jci.insight.131961
10. Xiong, G., Metheny, H., Johnson, B. N. & Cohen, A. S. A Comparison of Different Slicing Planes in Preservation of Major Hippocampal Pathway Fibers in the Mouse. *Front. Neuroanat.* **11,** 573–17 (2017).
11. Rafiq, A., DeLorenzo, R. J. & Coulter, D. A. Generation and propagation of epileptiform discharges in a combined entorhinal cortex/hippocampal slice. *J. Neurophysiol.* **70,** 1962–1974 (1993).
12. Jones, R. S. *et al.* Synaptic and intrinsic responses of medical entorhinal cortical cells in normal and magnesium-free medium in vitro. *J. Neurophysiol.* **59,** 1476–1496 (1988).
13. Stanton, P. K., Jones, R. S., Mody, I. & Heinemann, U. Epileptiform activity induced by lowering extracellular [Mg2+] in combined hippocampal-entorhinal cortex slices: modulation by receptors for norepinephrine and N-methyl-D-aspartate. *Epilepsy Res.* **1,** 53–62 (1987).
14. Walther, H., Lambert, J. D., Jones, R. S., Heinemann, U. & Hamon, B. Epileptiform activity in combined slices of the hippocampus, subiculum and entorhinal cortex during perfusion with low magnesium medium. *Neuroscience Letters* **69,** 156–161 (1986).
15. Bourgeois, E. B. *et al.* A Toolbox for Spatiotemporal Analysis of Voltage-Sensitive Dye Imaging Data in Brain Slices. *PLoS ONE* **9,** e108686–15 (2014).